EUKARYOTIC CELL, Feb. 2010, p. 288–305 Vol. 9, No. 2
1535-9778/10/$12.00 doi:10.1128/EC.00220-09

Distinct Subcellular Localization of a Group of Synaptobrevin-Like SNAREs in *Paramecium tetraurelia* and Effects of Silencing SNARE-Specific Chaperone NSF▽†

Christina Schilde, Barbara Schönemann, Ivonne M. Sehring, and Helmut Plattner*

Department of Biology, University of Konstanz, P.O. Box 5560, D-78457 Konstanz, Germany

Received 30 July 2009/Accepted 4 December 2009

We have identified new synaptobrevin-like SNAREs and localized the corresponding gene products with green fluorescent protein (GFP)-fusion constructs and specific antibodies at the light and electron microscope (EM) levels. These SNAREs, named *Paramecium tetraurelia* synaptobrevins 8 to 12 (PtSyb8 to PtSyb12), showed mostly very restricted, specific localization, as they were found predominantly on structures involved in endo- or phagocytosis. In summary, we found PtSyb8 and PtSyb9 associated with the nascent food vacuole, PtSyb10 near the cell surface, at the cytostome, and in close association with ciliary basal bodies, and PtSyb11 on early endosomes and on one side of the cytostome, while PtSyb12 was found in the cytosol. PtSyb4 and PtSyb5 (identified previously) were localized on small vesicles, PtSyb5 probably being engaged in trichocyst (dense core secretory vesicle) processing. PtSyb4 and PtSyb5 are related to each other and are the furthest deviating of all SNAREs identified so far. Because they show no similarity with any other R-SNAREs outside ciliates, they may represent a ciliate-specific adaptation. PtSyb10 forms small domains near ciliary bases, and silencing slows down cell rotation during depolarization-induced ciliary reversal. *NSF* silencing supports a function of cell surface SNAREs by revealing vesicles along the cell membrane at sites normally devoid of vesicles. The distinct distributions of these SNAREs emphasize the considerable differentiation of membrane trafficking, particularly along the endo-/phagocytic pathway, in this protozoan.

Paramecium tetraurelia is a unicellular organism that belongs to the ciliated protozoans and, thus, to the phylum *Alveolata*, which also comprises dinoflagellates and apicomplexans, such as the human pathogens *Toxoplasma* and *Plasmodium*. Like those organisms, *Paramecium* has to perform within one cell all functions that are normally shared between different cell types in multicellular organisms. Accordingly complex are the cytoskeletal anatomy (1), food uptake and processing (20), and membrane trafficking pathways (47). This complexity is mirrored in the mere size of the genome, with ~39,500 protein-coding genes (8). On this background we shall describe new genes and proteins—SNAREs, as defined below—of a superfamily contributing to specific membrane interactions. Together with previous studies (37, 52, 53) we may have now identified most of the SNARE genes in *Paramecium*. The large number of putative SNARE genes in *Paramecium* was unexpected and is similar to that in flowering plants (41) and mammals (39).

P. tetraurelia is a freshwater filter feeder that lives on bacteria and other small unicellular organisms. Food particles are transported into the oral cavity, first to the cytostome by action of cilia and then concentrated in the cytopharynx, where they are packaged into the nascent food vacuole. In parts of the oral cavity cilia display special arrangements, such as two peniculi and a quadrulus, and oral fibers emanate as rails for vesicle trafficking (3, 20). Vesicles of different sizes and origins travel close to the oral cavity and are frequently associated with the structures just mentioned. Once the food vacuole reaches a certain size, the nascent food vacuole is pinched off the cytopharynx and takes a defined route through the cytoplasm of the cell, termed cytoplasmic streaming or cyclosis (2), which is supported by specialized microtubule structures (54). Vesicles of an ~0.8-μm size (acidosomes) situated at the site of food vacuole formation at the cytopharynx fuse with the nascent food vacuole after it has detached from the cytopharynx, and they drastically lower the pH of the phagosome lumen (48). This may kill food bacteria, and it initiates a series of events leading to fusion of the digestive vacuole (phagosome) with lysosomes that deliver digestive enzymes for breakdown of digestible vacuole contents (20). The whole cycle of digestion is completed after ~20 min. Membranes and digestive enzymes are recycled from the digestive vacuole, and undigested waste products are excreted by fusion of the digestive vacuole at a specialized site on the cell surface, the cytoproct (2, 3). The membrane of the defecated vacuole is retrieved as ~100-nm discoidal vesicles and transported back along microtubular ribbons to the cytostome (2).

The whole cortex of *Paramecium* is a highly ordered structure with regularly arranged organelles (46). Soluble substances are ingested via permanent, regularly arranged ~0.1-μm large indentations at the cell surface, called parasomal sacs. These have a clathrin coat on their cytoplasmic side and correspond via small trafficking vesicles with the regularly arranged stationary early endosomes (terminal cisternae) situated beneath each ciliary basal body (3). There, different cargos are sorted into 100-nm vesicles that join the digestive pathways described above.

* Corresponding author. Mailing address: Department of Biology, University of Konstanz, P.O. Box 5560, D-78457 Konstanz, Germany. Phone: 49 7531 882228. Fax: 49 7531 882245. E-mail: helmut.plattner@uni-konstanz.de.

† Supplemental material for this article may be found at http://ec.asm.org/.

▽ Published ahead of print on 18 December 2009.

Paramecium also possesses dense core secretory vesicles called trichocysts, which are also regularly arranged in a fusion-competent stage at the cell surface. Each trichocyst docking site is surrounded by cortical calcium stores (alveolar sacs) (46). Trichocysts originate from the endoplasmic reticulum (ER) and undergo several stages of maturation until they achieve exocytosis competence (28).

Besides trichocysts and parasomal sacs (which may also participate in constitutive exocytosis [19]), no other sites of membrane delivery to the cell membrane are known up to now, as documented in the electron microscope (EM) image gallery presented by R. D. Allen at the website http:/www5.pbrc.hawaii.edu/allen/.

*S*oluble *N*-ethylmaleimide-sensitive factor *a*ttachment protein *re*ceptors (SNAREs) are of central importance to all membrane trafficking and have been found in every eukaryotic lineage investigated so far (25, 32, 39).The *N*-ethylmaleimide *s*ensitive *f*actor (NSF) is a SNARE-specific chaperone (32). SNARE molecules form a quarternary complex (SNARE complex) when they assemble to mediate membrane docking for subsequent fusion, with each one of the SNAREs containing one SNARE domain (synaptobrevin or syntaxin) or two (due to backfolding, as in SNAP-25 or related proteins; see below). The crystal structures of different SNARE complexes revealed conserved features that are now believed to be universal in all SNARE complexes (7, 17, 57, 63). Of the four SNARE helices forming a highly stable SNARE complex, three usually carry a glutamine (Q) residue and one carries an arginine (R) at the center of the SNARE domain; this is known as the "3Q + 1R rule" (17). Accordingly, SNAREs have been classified as Q- and R-SNAREs, and this nomenclature usually reflects the evolutionary origin of different types of SNARE proteins better than the old classification, as v- (*v*esicle) and t- (*t*arget) SNAREs. Q-SNAREs can be further subdivided into Qa-, Qb-, and Qc-SNAREs, with Qa-SNAREs often designated as syntaxins, whereas Qb- and Qc-SNAREs can be distinct proteins or both these SNARE domains can reside within a single protein, as in the case of the *syn*aptosomal-*a*ssociated *p*rotein of *25* kDa (SNAP-25). R-SNAREs, like synaptobrevins or the *t*etanus toxin-*i*nsensitive *v*esicle-*a*ssociated *m*embrane *p*rotein (TI-VAMP), are often situated on the vesicle side and have been subdivided, referring to their length, into brevins and longins (with a longer N-terminal cytosolic stretch). Because the tetanus toxin-sensitive brevins so far have been found only in metazoans and yeast, the more widespread tetanus toxin-insensitive longins have to be considered the ancestral R-SNAREs. Longins are characterized by their conserved longin domain structure, a fold that is similar to a profilin-like fold (18, 49, 50). As found with Sec22, a longin occurring not only in organisms from yeast to mammals but also in *Paramecium* (37), the longin domain, depending on its folding state, contributes to vesicle formation in the endoplasmic reticulum and further targeting (44).

There are exceptions to some of these rules, e.g., there are SNAREs with a central amino acid other than an R (or Q) residue in the zero layer. Nevertheless, the repetitive arrangement of typical amino acids (heptad repeats, relevant for SNARE complex formation) around the zero layer, as characteristic of a SNARE domain, in combination with additional criteria, still allows one to identify such proteins as SNAREs. We have used a bioinformatic approach in the present work (see below).

We previously identified a set of R-SNAREs (53), Q-SNAREs (37), and a SNAP-25 homolog (52) in *P. tetraurelia*. Here, we identified by sequence homology, either of defined domains or of the overall structure, a group of related synaptobrevin-like SNAREs which we investigated in more detail, including their subcellular localization. In contrast to the *Paramecium* R-SNAREs previously described (53), those newly described here all have an unorthodox amino acid, Asp or rarely His, in the zero layer of their SNARE domain, and only two of them possess a longin domain. We found that all these new SNAREs show distinct subcellular localizations, and we found that a great number of them are associated with food vacuole processing or endosomal trafficking. Some of the synaptobrevin-like SNAREs investigated here show an identical distribution pattern, as previously found for specific Qa-SNAREs (37), and thus they could be constituents of the same SNARE complexes.

MATERIALS AND METHODS

Cell culture. The *P. tetraurelia* wild-type strains used were 7S and d4-2, both derived from stock 51S (56). Cells were cultivated in a bacterially inoculated medium as described previously (38). For staining of acidic vesicles, starved cells in piperazine-*N*,*N*′-bis(2-ethanesulfonic acid) (PIPES) buffer (5 mM PIPES, 1 mM KCl, 1 mM $CaCl_2$, pH 7.0) were incubated for 10 min with 100 nM LysoTracker Red DND-99 (Molecular Probes Eugene, OR).

Annotation and characterization of Pt*syb* genes. In order to identify new SNARE genes in *Paramecium* (Pt*syb*) by homology searches, the *Paramecium* database (http://paramecium.cgm-cnrs-gif.fr) was screened by using the nucleotide and amino acid sequences of R-SNAREs from already-annotated *Paramecium* Pt*syb* genes. In a parallel approach, the SNARE database (39) was searched for annotated *P. tetraurelia* SNAREs. Positive hits were further analyzed by performing BLAST searches with the NCBI database (6). Conserved motif searches were performed with either PROSITE (9) or with the SNARE database (39). We also used PSIPRED (34) and MEMSAT 2 (33, 35), two methods for secondary structure and transmembrane topology prediction, respectively, included at the server at http://bioinf.cs.ucl.ac.uk/psipred/ (45).

PCR of genomic DNA and cDNAs. Total wild-type DNA from strain 7S for PCR was prepared from log-phase cultures as described by Godiska et al. (23). The open reading frames (ORFs) of individual Pt*syb* genes were amplified by reverse transcriptase (RT)-PCR using total RNA prepared according to the methods of Haynes et al. (31). RT-PCR was performed in a programmable thermocycler T3 (Biometra, Göttingen, Germany) using a 3′-oligo(dTT) primer and the SuperScript III reverse transcriptase (Invitrogen, Karlsruhe, Germany) for first-strand cDNA synthesis [3′-oligo(dTT) primer, 5′-AACTGGAAGAAT TCGCGGCCGCGGAATTTTTTTTTTTTTT-3′]. The subsequent PCR (50-μl reaction volume) was performed with the Advantage 2 cDNA polymerase mix (Clontech, Palo Alto, CA) using Pt*syb*-specific oligonucleotides (see Table SA in the supplemental material) with or without the artificial restriction sites SpeI/XhoI or XbaI/XhoI added at their 5′ ends. In general, amplifications were performed with one cycle of denaturation (95°C, 1 min), 40 to 42 cycles of denaturation (95°C, 30 s), annealing (54 to 58°C, 45 s), and extension (68°C, 3 min), followed by a final extension step at 68°C for 5 min. PCR products were subcloned into the plasmid pCR2.1 by using the TOPO-TA cloning kit (Invitrogen) according to the manufacturer's instructions. After transformation into *Escherichia coli* (TOP10F′) cells, positive clones were sequenced as described below.

Sequencing. Sequencing was performed by the MWG Biotech (Martinsried, Germany) custom sequencing service. DNA sequences were aligned by the ClustalW feature integrated in the Lasergene software package (DNASTAR).

Construction and microinjection of GFP expression plasmids. Pt*syb*-specific PCR products obtained with the oligonucleotides listed in Table SA of the supplemental material were cloned into the enhanced GFP (eGFP) expression plasmid pPXV-GFP (27) either in front of the eGFP gene, as described by Wassmer et al. (60), or at the end of the eGFP gene between one of the restriction sites SpeI or XbaI, and the XhoI site, respectively, of the plasmid by using conventional cloning procedures (51). For microinjection of cells, the

TABLE 1. Molecular characteristics of PtSNARE genes and derived protein sequences of this study

Gene	Accession no.	Scaffold no.	DNA properties				Protein properties						
			Length (bp)	ORF (bp)	No. of introns	% Identity[a]	Length (aa)	Size (kDa)	% Identity[a]	Longin (aa)	SNARE domain (aa)	Transmembrane (aa)	Localization
Pt*syb4-1*[b]	CAK60380	12	648	603	2		200	23.7				168–190	Unknown compartment
Pt*syb4-2*[b]	CAK94759	97	645	594	2	75.4	197	23.3	59.1	2–64		174–191	Unknown compartment
Pt*syb5-1*[b]	CAK73681	26	528	504	1		167	19.3		2–68		145–164	Unknown compartment
Pt*syb8-1*[b]	CAK63760	138	764	684	3		227	26.0		9–100	137–189	202–221	Cytopharynx
Pt*VAMP741*	CAK73918	266	1,186	1,069	4		363	41.8		159–250	287–339	252–371	ND[c]
Pt*syb9-1*[b]	CAK63650	137	789	663	5		228	26.8		8–96	131–191	197–216	Cytopharynx
Pt*syb9-2*[b]	CAK73996	27	788	663	5	62.4	220	25.7	84.6	8–97	131–191	197–216	
Pt*syb10-1*[b]	CAK90226	78	688	666	1		221	25.1			141–192	198–220	Ciliary basis
Pt*syb10-2*	CAK88554	70	691	621	3	86.4	202	23.4	81.0		131–178	183–205	
Pt*syb11-1*[b]	CAK75272	3	746	669	2		222	25.7			138–190	202–221	Early endosomes
Pt*syb11-2*	CAK85181	6	714	663	2	81.1	220	25.6	85.2		129–188	200–219	Early endosomes
Pt*syb12-1*[b]	CAK87252	66	557	507	2		168	19.5					Cytosol

[a] Sequences were aligned by the Clustal W method.
[b] Genes were also analyzed on the cDNA level.
[c] ND, not determined.

pPXV-GFP fusion plasmids were linearized with SfiI (New England Biolabs, Frankfurt, Germany), which cuts between the *Tetrahymena thermophila* inverted telomeric repeats, thus helping to stabilize the DNA in the macronucleus after injection (30). DNA to be injected was isopropanol precipitated and resuspended to a concentration of 1 to 5 μg/μl in MilliQ water. For microinjection, we used postautogamous cells, which were allowed to grow for three to four generations in bactererially preinoculated salad medium. To avoid any disturbances of the transformation process, cells were also treated with 0.2% aminoethyldextran (to remove trichocysts) and equilibrated in Dryl's buffer (2 mM sodium citrate, 1 mM NaH_2PO_4, 1 mM Na_2HPO_4, 1.5 mM $CaCl_2$, pH 6.8 [16]) supplemented with 0.2% bovine serum albumin (BSA). DNA microinjections were made with glass microcapillaries under an Axiovert 100TV phase-contrast microscope (Zeiss, Oberkochen, Germany). Expression of GFP-fusion proteins in clonal descendants of microinjected cells was analyzed after 16 h to 48 h by epifluorescence microscopy in an Axiovert 100TV microscope equipped with GFP filter set 13, a plan Neofluar 40× oil immersion objective (numeric aperture, 1.30), and with a ProgRes C10 plus camera system from Jenoptik (Jena, Germany). Excitation light was produced by a 100-W HBO lamp (Osram, Munich, Germany). Images were processed and arranged with Adobe Photoshop (Adobe Systems, San Jose, CA).

Posttranscriptional gene silencing of PtSyb10. A fragment of 126 bp (bp 175 to 300) of identical sequence between both PtSyb10 isoforms was chosen for preparing a gene silencing construct. The silencing sequence was contained in the double T7 promoter plasmid pPD. To monitor successful silencing, we applied the plasmid pPD-nd7 (nondischarge), causing trichocyst exocytosis incompetence (55). For a more detailed description of this methodology, see reference 21. The RNase III-deficient *E. coli* strain HT115 (58) was transformed with these constructs and used for silencing by feeding as described previously (60).

After silencing by feeding with transformed *E. coli* (>48 h) and provided that adequate results were achieved with parallel controls (exocytosis deficiency with an nd7-containing vector), silenced cells contained in a medium with 5 mM PIPES buffer (pH 7.0) with KCl and $CaCl_2$ added at 1 mM each were evaluated based on electronic recordings according to the following criteria. We determined (i) the length of cilia on the somatic cell surface as seen in the phase-contrast microscope. On randomly chosen snapshots of median cell planes we measured the length of cilia at sites where they were oriented perpendicular to the cell surface. (ii) With time-lapse analysis we determined the normal swimming speed (forward movement) of cells. When randomly chosen, straight forward-swimming cells could be followed on a linear track over at least several tens of micrometers; the actual travel distance was then references to the time elapsed. (iii) After depolarization with 10 mM KCl, the frequency of cell rotations during ciliary reversal was determined. This was performed by counting rotations (recognized by the rotation of any structural landmark, such as the cytostome, contractile vacuoles, etc.) per second in low-speed playback. (iv) Western blot assays with antibodies against PtSyb10 were performed as described previously (53) using tubulin, demonstrated with the anti-tubulin antibody indicated below, as a loading control. All data were references to controls with the respective vector (empty pPD or nd7) and analyzed by Sigma Plot (Systat Software Inc., San Jose, CA) for mean values, standard errors of the means (SEM), and significance values by Student's *t* test. Values presented in Table 2, below, were randomly collected from three sets of experiments, all showing the same tendency with regard to the parameters analyzed.

Expression of PtSyb-specific peptides in *E. coli*. For heterologous expression of PtSyb-specific peptides, we selected the N-terminal part of the coding region preceding the transmembrane domain of PtSyb8-1 (amino acids [aa] 1 to 205; emb CAK63760), PtSyb9-1 (aa 1 to 195; emb CAK63650), and PtSyb10-1 (aa 1 to 198; emb CAK90226). After changing all deviating *Paramecium* glutamine codons (TAA and TAG) into universal glutamine codons (CAA and CAG) by PCR methods (14) (for primers, see Table SA in the supplemental material), this region of Pt*syb* genes was cloned into the NcoI/XhoI restriction sites of the pRV11 expression vector (62), a derivative of the pET system from Novagen (Madison, WI), which adds a 6-amino-acid peptide to the C terminus of the selected sequence, including a hexahistidine tag for purification of the recombinant peptides.

Purification of a recombinant PtSyb peptides and preparation of polyclonal antibodies. The recombinant PtSyb peptides were purified by affinity chromatography on Ni^{2+}-nitrilotriacetate agarose under denaturing conditions, as recommended by the manufacturer (Novagen). The recombinant peptides were eluted with a buffer at pH 4.5 containing 100 mM NaH_2P0_4, 10 mM Trizma base supplemented with 8 M urea and 1 M imidazole. The collected fractions were analyzed on SDS-polyacrylamide gels, and those containing the recombinant peptides were pooled, dialyzed against phosphate-buffered saline (PBS), and used for immunization of rabbits. Before this, rabbits of a large departmental pool were routinely controlled for suitability, i.e., for the absence of any secondary antibody staining in Western blot assays and in immunofluorescence assays. After several boosts, positive sera were taken and affinity purified by two subsequent chromatography steps as described previously (38).

Immunofluorescence analysis. Cells suspended in PIPES-HCl buffer (5 mM, pH 7.2) with 1 mM KCl and 1 mM $CaCl_2$ were fixed in 4% (wt/vol) freshly depolymerized formaldehyde in PBS solution plus 1% Triton X-100 (Sigma, Taufkirchen, Germany) for 20 min at 20°C, washed twice in PBS, then incubated in PBS supplemented with 50 mM glycine for 10 min, and finally in PBS plus 1% BSA. Occasionally, as indicated in the respective figure legends, cells overexpressing a SNARE-GFP fusion protein were also fixed for subsequent immunofluorescence in analogy to EM samples. Samples were then exposed to affinity-purified anti-PtSyb antibodies (1:50; ~20 μg/ml), followed by Alexa Fluor 488-conjugated anti-rabbit antibodies (Molecular Probes), the latter diluted 1:100 (~10 μg/ml) in PBS plus 1% BSA. Tubulin structures were stained with mouse monoclonal antibody against α-tubulin (clone DM1A; Sigma), followed

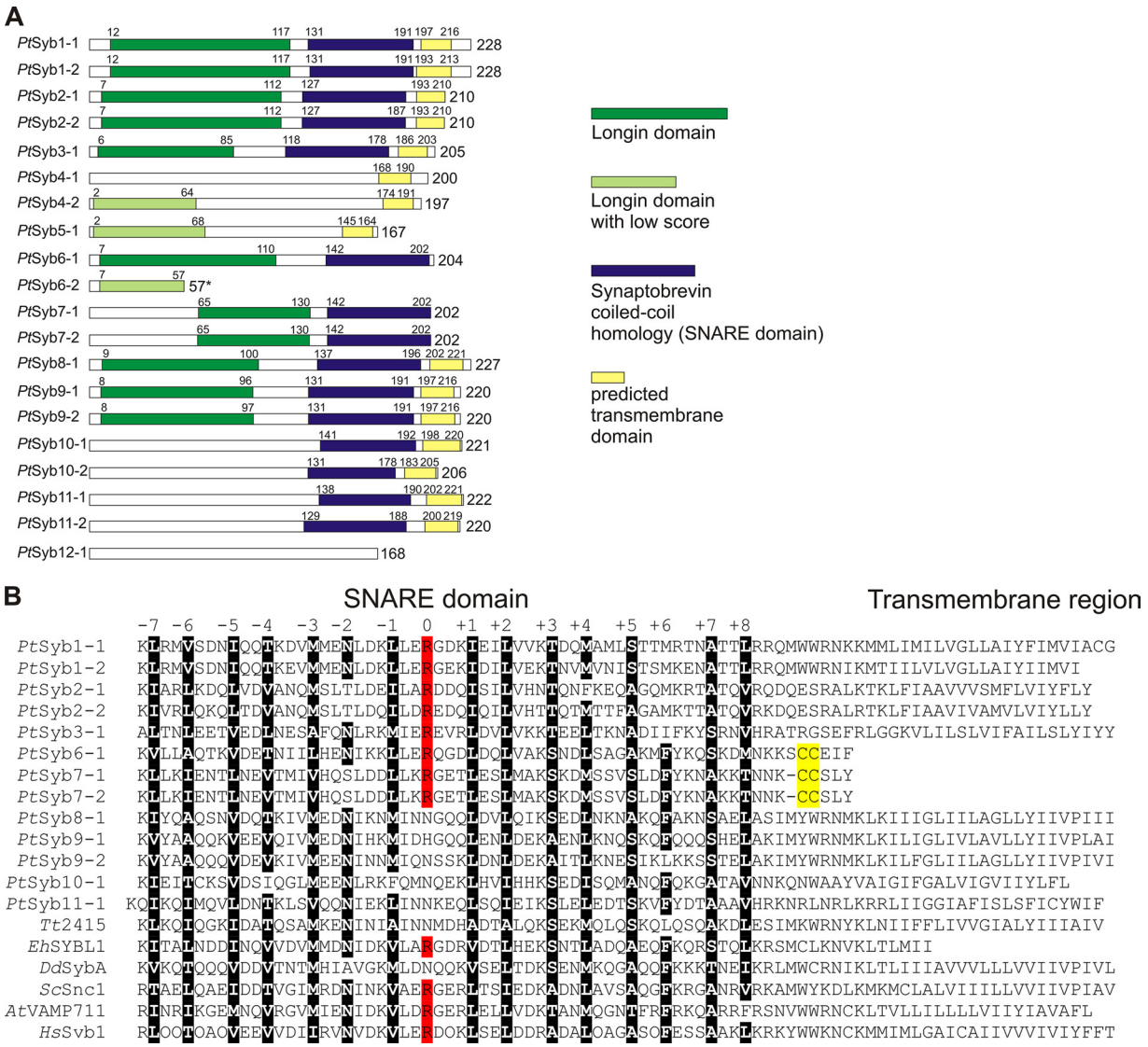

FIG. 1. Sequence analysis of *P. tetraurelia* synaptobrevins. (A) Domain structure of PtSybs based on homology to known proteins and identified longin (green), synaptobrevin (blue), and transmembrane (yellow) domains. Pt*Syb6-2* produces a truncated protein because of the creation of a stop codon by intron splicing (*). (B) Alignment of the SNARE domains and predicted transmembrane domains obtained by using ClustalW (slow, accurate) analysis of *Paramecium* synaptobrevins, a *Tetrahymena thermophila* synaptobrevin homolog (Tt2415; TIGR gene identifier 2415), *Entamoeba histolytica* synaptobrevin-like protein 1 (EhSYBL1; GenBank accession number AY256852), *Dictyostelium discoideum* SybA (Dictybase identifier DDB0214903), *Saccharomyces cerevisiae* Snc1 (GenBank accession number AAC05002), *Arabidopsis thailiana* VAMP711 (GenBank accession number O49377), and *Homo sapiens* Syb1 (GenBank accession number AAA60603). Conserved heptad repeats are shown in black. Note that the orthodox zero-layer arginine (red) is not present in all PtSybs. The 17- to 24-amino-acid-long transmembrane domains are absent from PtSyb families 6 and 7; instead, these proteins possess a potential carboxy-terminal putative prenylation/palmitoylation motif (yellow).

by Alexa Fluor 594-conjugated anti-mouse antibodies (1:100; Molecular Probes). For controls, either preimmune serum was used or primary antibodies were omitted, resulting in an extremely weak background. Samples were mounted with Mowiol supplemented with *n*-propylgallate to reduce fading. Fluorescence was analyzed in a confocal laser-scanning LSM 510 microscope (Zeiss) equipped with a Plan-Apochromat 63× oil immersion objective (numerical aperture, 1.4) or in a conventional epifluorescence microscope (described above). Images acquired with the LSM 510 software were further processed with Photoshop software (Adobe Systems).

Immuno-EM analysis. *Paramecium* wild-type cells and cells transformed with GFP–PtSyb10-1 or with GFP–PtSyb5-1 were fixed in 4% formaldehyde plus 0.15% glutaraldehyde in 100 mM cacodylate buffer, pH 7.0, for 2.5 h at room temperature, followed by two washes with the same buffer. Cells were dehydrated in an ethanol series and embedded in LR-Gold resin (Agar Scientifique, Stansted, United Kingdom) according to standard protocols, including UV polymerization at −35°C. Sections were incubated with anti-GFP antibodies (61) or anti-PtSyb8 or anti-PtSyb9 antibodies, followed by protein A bound to colloidal gold particles of 5 nm (protein A-Au_5), stained with aqueous uranyl acetate, and analyzed in a Zeiss EM10, all as previously described (38). For controls, either preimmune serum was used or primary antibodies were omitted, or sections were incubated with antibodies against irrelevant (human) antigens at a high concentration, all resulting in a very low number of loosely scattered gold granules.

NSF silencing and ultrastructural analysis. Cells were silenced in NSF for the maximum time tolerated by the cells (≥35 h) as described above for Pt*syb10*. For routine EM analysis the same procedure as used by Kissmehl et al. (36) was applied. This included fixation with 1% OsO_4, embedding in Spurr's resin, and evaluation of ultrathin sections stained with aqueous uranyl acetate and lead citrate, pH 12.0. In controls, using samples without silencing but following the

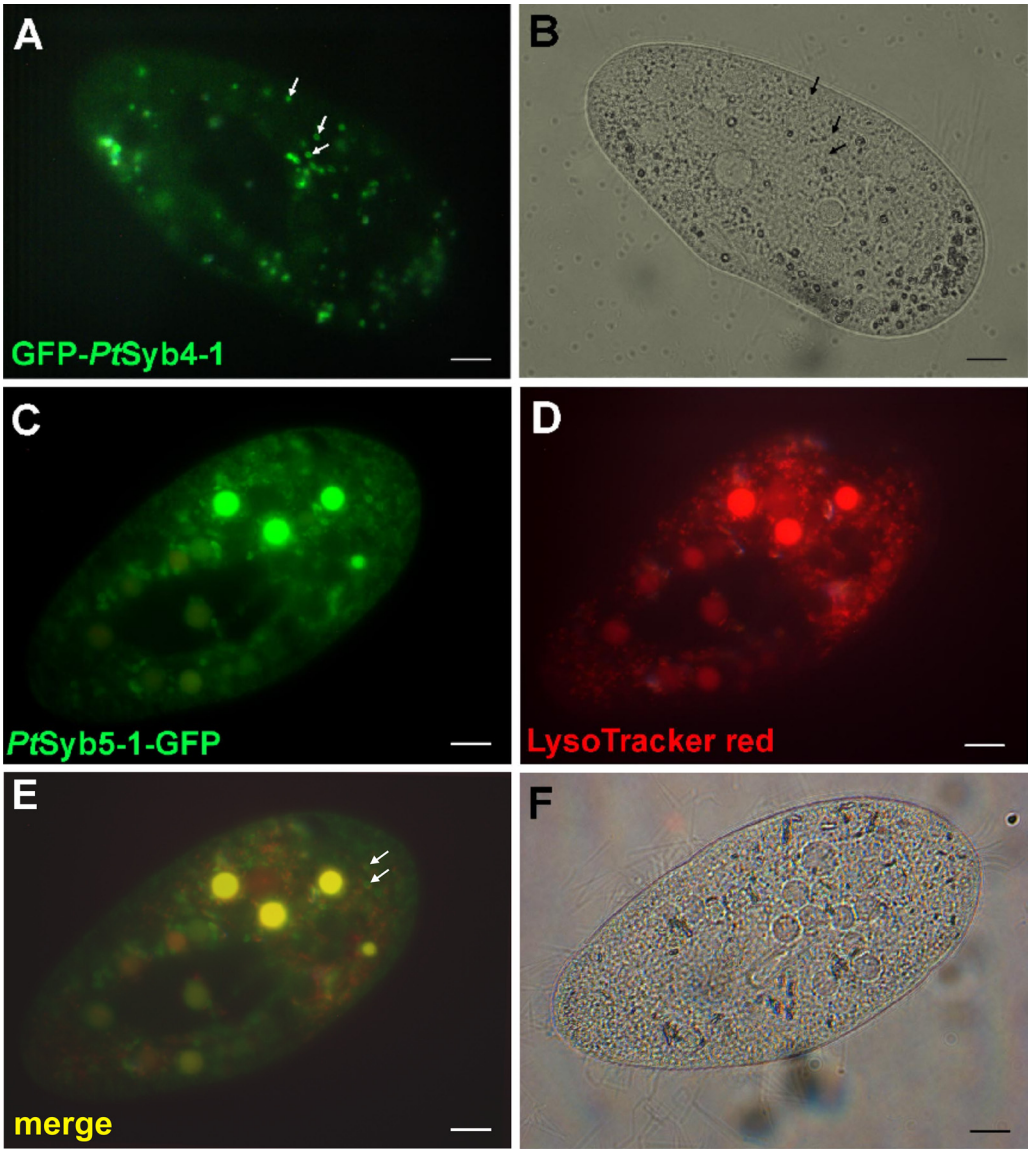

FIG. 2. Localization of PtSyb4-1 and PtSyb5-1 as GFP-fusion proteins in vesicles undergoing cyclosis. (A and B) Epifluorescence (A) and bright-field (B) images of a living cell expressing GFP–PtSyb4-1. Arrows indicate GFP-marked small vesicles. (C and D) Epifluorescence of a living cell expressing PtSyb5-1–GFP double stained with LysoTracker red (D). (E) The merged image of panels C and D, PtSyb5-1–GFP with LysoTracker red staining, shows no indication of colocalization of PtSyb5-1–GFP–positive vesicles (e.g., at arrows) with acidic vesicles (pH $\leq$ 5.2). Note that three of the food vacuoles show strong autofluorescence in both fluorescence channels. (F) Corresponding bright-field image of the same cell. Note that the cell has moved a little between the image capture and has extruded trichocysts which are visible as thin rods surrounding the cell. Bars, 10 μm.

same preparation protocol, no structural alterations were seen, as described below for NSF silencing. Such images of the cell cortex corresponded to the numerous ones published elsewhere, e.g., at the website http:/www5.pbrc.hawaii.edu/allen/.

RESULTS

Molecular identification of new SNARE homologs in *P. tetraurelia*. In Table 1 we characterize genes of the synaptobrevin-related PtSNARE subfamilies addressed in the current paper and the domain structure of the corresponding gene products. Some of the SNAREs contained here, subfamilies PtSyb4, PtSyb5, PtSyb8, and PtSyb9, had already been identified by us previously (53). However, only now can we present some more concise molecular characteristics (Fig. 1) and data on their localization and, thus, derive some functional aspects, in addition to the newly described subfamilies PtSyb10, PtSyb11, and PtSyb12.

The PtSyb4 and PtSyb9 subfamilies consist of two isoforms each: PtSyb4-1 and PtSyb4-2 as well as PtSyb9-1 and PtSyb9-2. Subfamilies PtSyb5 and PtSyb8 are represented by only a single isoform. The synaptobrevin-related proteins PtSyb4-2 and PtSyb5-1 contain a very weakly conserved longin-like fold but no recognizable SNARE domain. However, they share sequence homology to PtSyb3-1 and were therefore included in

the R-SNARE family of *P. tetraurelia* (53). The subfamilies PtSyb8 and PtSyb9 lack the conserved arginine of the SNARE motif zero layer but do not possess a glutamine typical of Q-SNAREs at this position either. However, the homology to the R-SNARE longin domain of PtSyb8 and overall sequence homology of the PtSyb9 isoforms to other PtSybs clearly places them in the longin-type family of R-SNAREs (53).

The newly developed SNARE database (http://bioinformatics.mpibpc.mpg.de/snare/index.jsp) (39), which contains an algorithm trained to recognize certain features of SNARE motifs and a collection of SNARE protein sequences classified by HMM profiles, identified two additional R-SNARE homologs in the *P. tetraurelia* genome, which we named, following our previous nomenclature, PtSyb10-1 (emb CAK90226) and PtSyb11-1 (emb CAK75272), respectively. Closer analysis of the openly available *P. tetraurelia* genome sequence (http://paramecium.cgm.cnrs-gif.fr) revealed that both PtSyb10-1 and PtSyb11-1 possess closely related sister isoforms (ohnologs), named PtSyb10-2 (emb CAK88554) and PtSyb11-2 (emb CAK85181), respectively. We also identified another protein related to the PtSyb11 subfamily, which we named PtSyb12-1 (emb CAK87252) and which does not have any sister isoform. PtSyb12-1 is identical to an automatically annotated *P. tetraurelia* hypothetical protein. It has no homologs in other species and contains neither a recognizable SNARE motif nor a transmembrane domain (39). Interestingly, the SNARE database (39) additionally identified an R-SNARE with close homology to PtSyb8-1, named VAMP741 (emb CAK73918), that by closer inspection seems to contain the complete reading frame of Pt*syb8-1* within a larger open reading frame but does not lie on a corresponding sister scaffold from the last whole-genome duplication (8) and hence is not a sister isoform to Pt*syb8-1*. Furthermore, the copy of Pt*syb8-1* in *VAMP741* lies in an inverse orientation exactly at the beginning of scaffold 266, and the open reading frame of *VAMP741* also contains a "like-Sm ribonucleoprotein-related protein" domain. This suggests that *VAMP741* is not a protein-encoding gene, but scaffold 266 might contain an artificial fusion at the end. All new genes, apart from *VAMP741*, Pt*syb10-2*, and Pt*syb11-2*, were verified on the genomic and cDNA levels and confirmed the automatic annotation of the *P. tetraurelia* genome project (http://paramecium.cgm.cnrs-gif.fr).

Table 1 shows that, by nucleotide sequence, paralogs of Pt*syb9* to Pt*syb11* differ from each other by only ~15%. Table 1 also indicates introns of a small size as characteristic of *Paramecium* (8). On an amino acid level all PtSyb proteins described are widely different from PtSyb1, as previously described (53). Their domain structure and zero-layer amino acids are briefly summarized in Table 1 and Fig. 1 and reveal wide variations. This concerns the presence or absence of a longin domain (PtSyb8 and PtSyb9 versus PtSyb10 and PtSyb11) and replacement of Arg by Asp (PtSyb8, PtSyb9-2, PtSyb10, and PtSyb11) or His (PtSyb9-1) in the zero layer of the SNARE domain. For the questionable identity of PtSyb12, see below. The subcellular localization of the newly described PtSNAREs, explored below, is summarized in the scheme at the end of this article.

PtSyb4 and PtSyb5 are associated with small vesicles. To assess the native subcellular localization of PtSyb4-1 and PtSyb5-1, we constructed an N-terminal GFP-fusion of PtSyb4-1 (GFP–PtSyb4-1) and a C-terminal GFP-fusion for

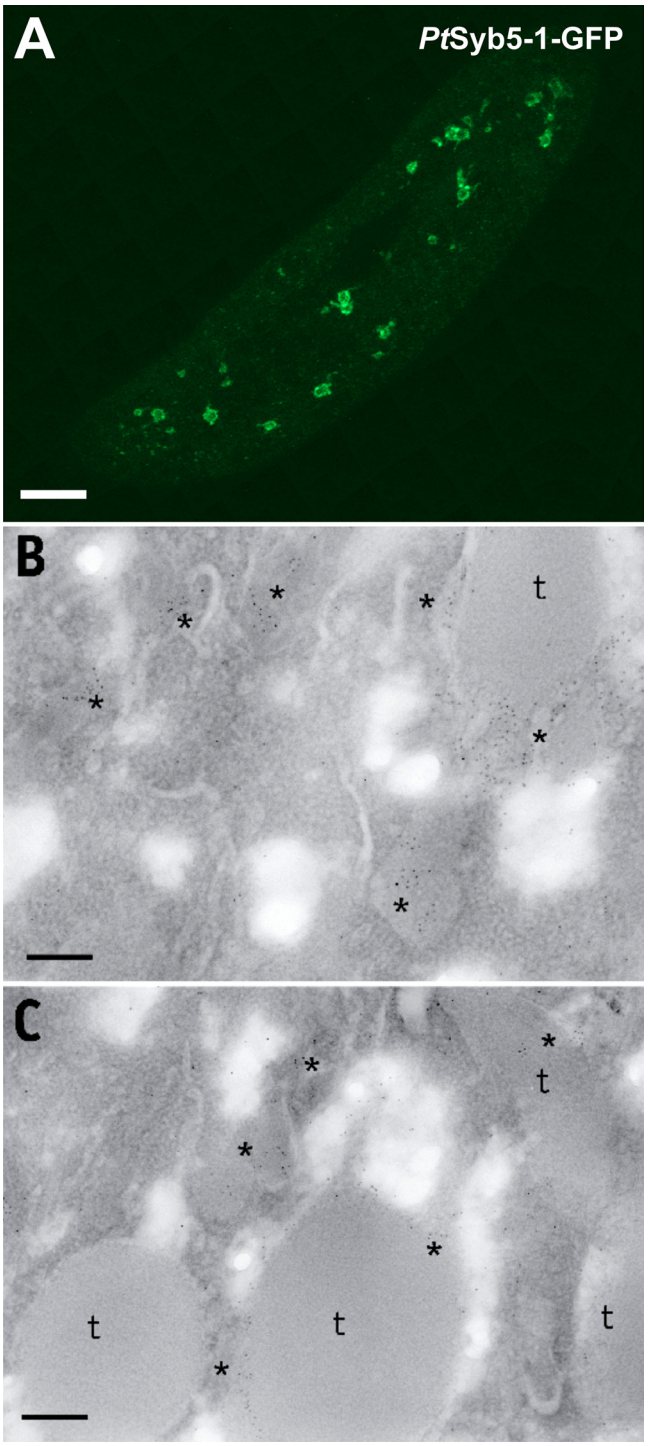

FIG. 3. Localization of PtSyb5-1–GFP after fixation on the light microscopic (A) or on the EM (B and C) level. (A) Stack reconstruction of a confocal image series from a fixed PtSyb5-1–GFP cell showing GFP fluorescence on the membrane of numerous small misshapen vesicles. Bar, 10 μm. (B and C) Two examples of EM images of detection of GFP by anti-GFP antibody/protein A-Au_5 conjugate in PtSyb5-1–GFP–expressing cells show labeling surrounding undocked trichocysts (t), mainly associated with structures (asterisks) of identical texture as trichocysts. For details, see the text. Bars, 250 nm.

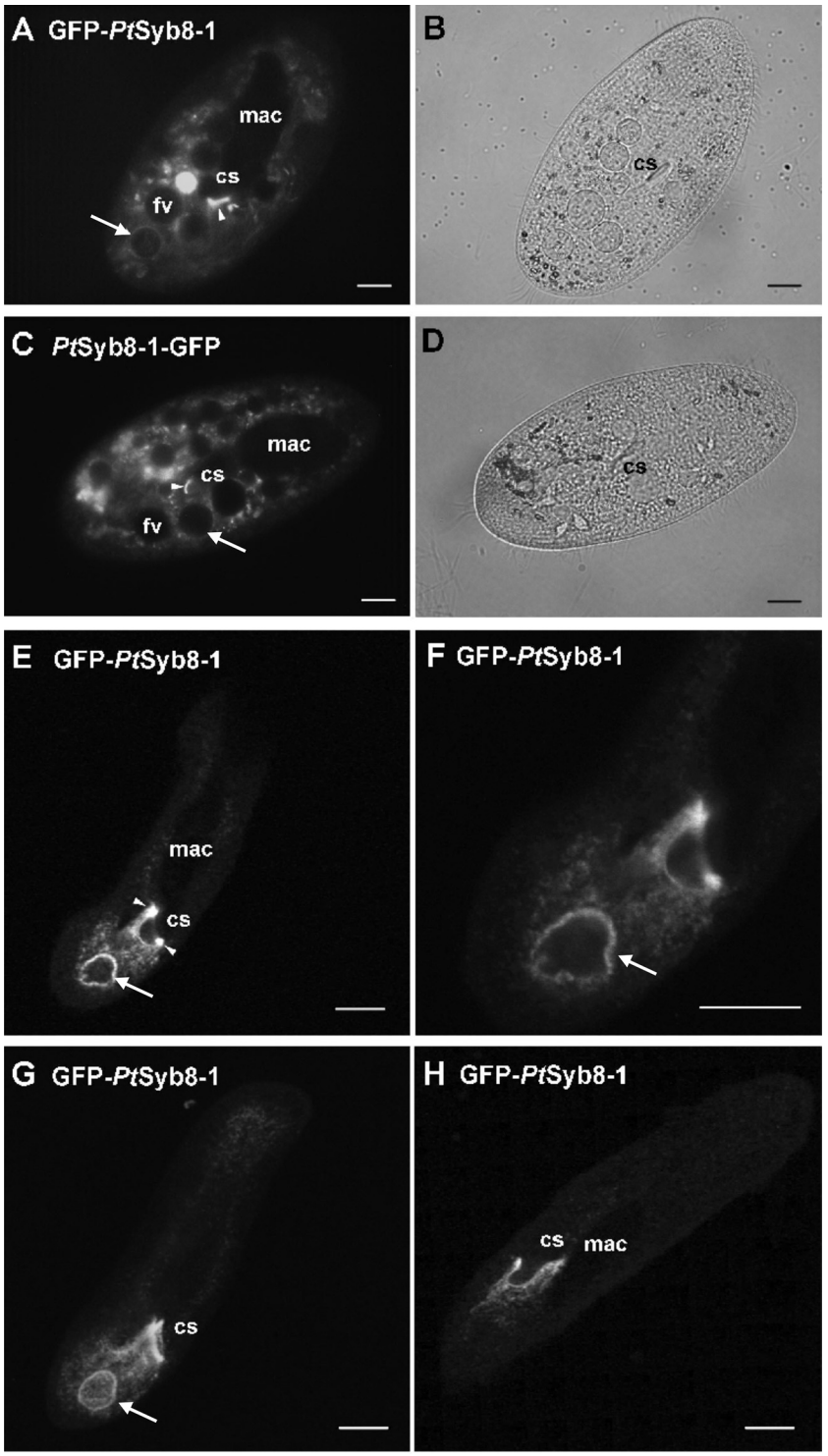

FIG. 4. Localization of PtSyb8-1–GFP–fusion constructs. (A and C) GFP–PtSyb8-1 (A) and PtSyb8-1–GFP (C) stain a crescent-shaped structure at the cytopharynx (arrowheads). There was also some staining on the membrane of a single food vacuole (fv; arrows). Note that the bright labeling of the big vacuole in panel A is an artifact due to fluorescence of vacuole contents. (B and D) Corresponding bright-field images of the living cells. (E to H) 3D reconstruction of confocal image stacks (1-μm thickness) from a fixed GFP–PtSyb8-1 cell shows strong staining at the cytopharynx (arrowheads) and of the surface of a previously internalized food vacuole (arrows). (F) Enlargement from panel E. In some images trains of intensely labeled small vesicles leading to the cytopharynx are visible. cs, cytostome; mac, macronucleus. Bars, 10 μm.

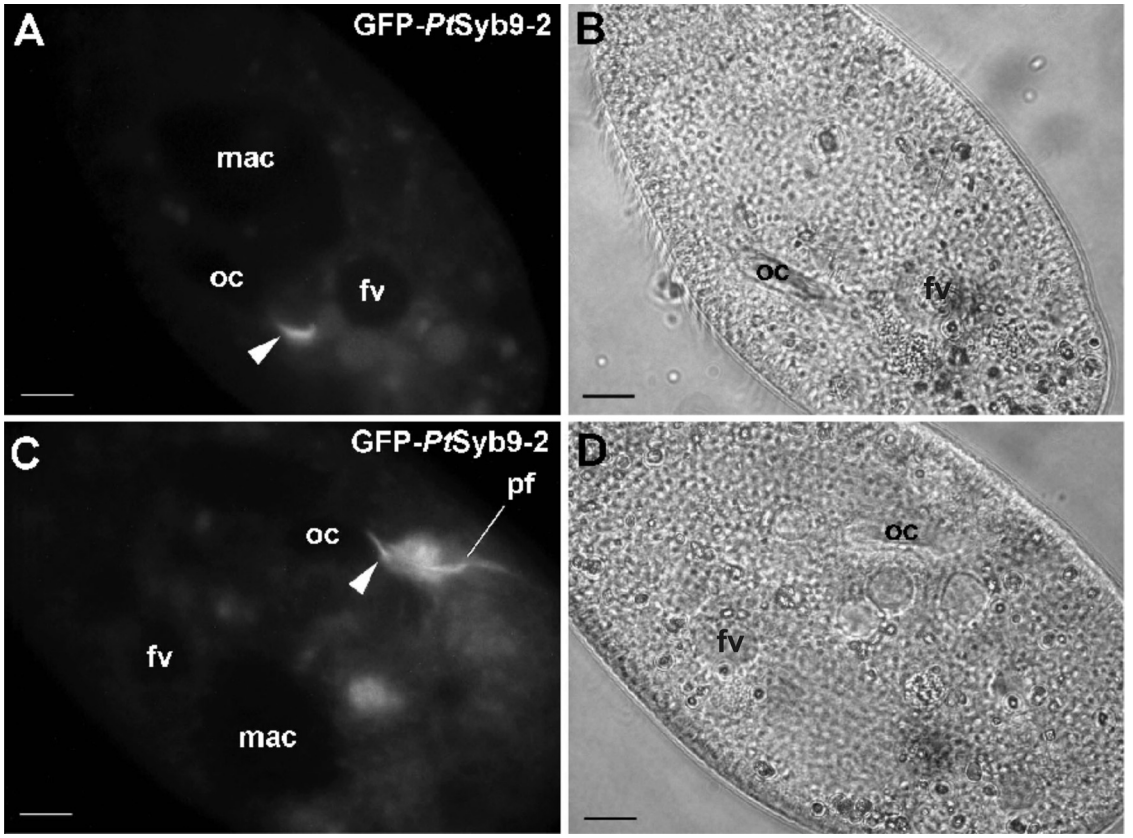

FIG. 5. Localization of GFP–PtSyb9-2 in living cells. (A and C) GFP–PtSyb9-2 stains the crescent-shaped site of nascent food vacuole formation at the cytopharynx (arrowheads) as well as the postoral fibers (pf) (C), structures involved in steering the newly formed food vacuole toward the posterior end of the cell. The oral cavity (oc) itself, the macronucleus (mac), and food vacuoles (fv) are not stained. (B and D) Corresponding bright-field images. The anterior end of the cell is oriented toward the top left of the images. Bars, 10 μm.

PtSyb5-1 (PtSyb5-1–GFP) and expressed them in *P. tetraurelia*. In both cases, strong staining of the membrane of numerous small round vesicles of constant size, ~1 μm in diameter, was observed (Fig. 2A and C). These vesicles moved with the cyclosis stream, but sometimes they were observed cohering in clusters. The GFP-positive vesicles were clearly distinct from crystal inclusions of the cells, as the corresponding areas in transmission light appeared completely devoid of any structures resembling crystals, which otherwise can be easily identified (Fig. 2B and F). Double staining of live GFP-PtSyb5-transfected cells with LysoTracker red (Fig. 2C and D) revealed no, or no consistent, colocalization of acidic vesicles with the GFP-stained vesicles (Fig. 2E). Thus, the GFP–PtSyb4-1- and PtSyb5-1–GFP–stained vesicles are different from phago-/lysosomal components undergoing cyclosis.

After formaldehyde fixation, the clustered small vesicles containing PtSyb5-1–GFP show fluorescence (Fig. 3A) compatible with the anti-GFP antibody/protein A-gold (Au_5) labeling in the EM images (Fig. 3B and C). The gold label is intimately associated with structures of irregular shape, recalling those in the fluorescence images, apposed to "free" (undocked) trichocysts, and they display the same typical structure of the trichocyst secretory materials. Notably, PtSyb5 is a likely candidate for the so-far-unidentified R-SNARE of trichocysts, which here became visible by overexpression as a GFP-fusion protein. Thus, PtSyb4 and PtSyb5 may belong to components of two different membrane sorting pathways (see also Discussion).

Controls to immunolocalizations. Specificity of immunofluorescence localization was controlled at different levels (see Materials and Methods). Before immunization, rabbits were routinely controlled for suitability, i.e., for the absence of any staining with the preimmune serum in Western blot assays and in immunofluorescence. Another control was to probe the peptide antigen (e.g., residues 1 to 205 of PtSyb8, to which antibodies were generated), and in parallel cell homogenates, in Western blot assays with antibodies (see Fig. SA-a in the supplemental material). The peptide, 24 kDa in size, is detected by anti-PtSyb8-1 antibodies. In homogenates a stronger band of slightly larger size (26 kDa) and a weaker band of smaller size (~22 kDa) is detected, the larger one corresponding to the size of the endogenous PtSyb8 molecule and the smaller one to a proteolytic degradation product.

Also as controls, primary antibodies were omitted in fluorescence immunolocalization, while labeled second antibodies were applied (see Fig. SA-b in the supplemental material). No label was recognized. EM studies included exposure of ultrathin sections to the same type of gold label, i.e., protein A-Au_5, as we used throughout the present study, but without previous incubation with a primary antibody or, as an even more strin-

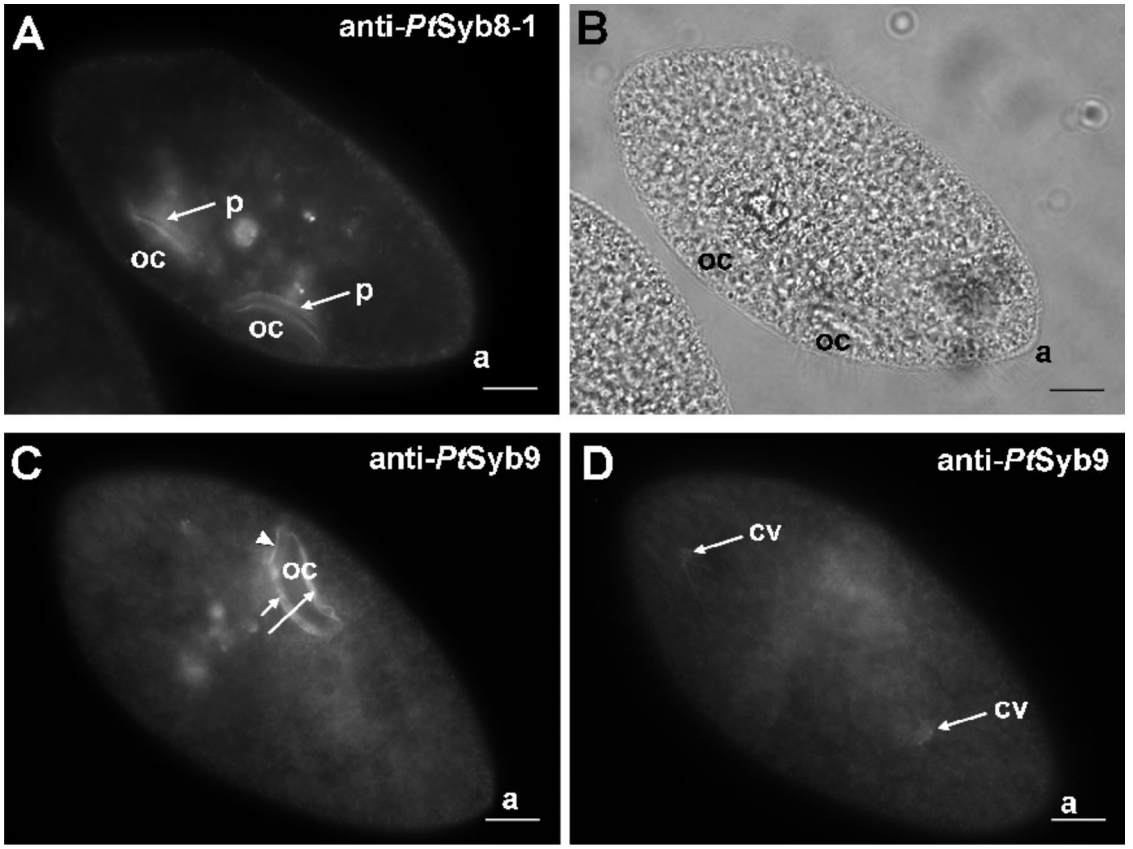

FIG. 6. Anti-PtSyb8-1 and anti-PtSyb9 antibody staining. (A) A specific antibody against PtSyb8-1 shows strong staining of the peniculi (p) lining the oral cavity (oc). The image shows two cytostomes of a dividing cell. a, the anterior end of the cell. (B) Bright-field image of the same cell. (C) An anti-PtSyb9 antibody stains vesicles along the oral cavity (oc; arrows) as well as the site of nascent food vacuole formation (arrowhead). (C and D) The anti-PtSyb9 antibody also exhibits a rather faint staining of the contractile vacuole system (cv) and some staining at the cell surface. Bars, 10 μm.

gent control, with previous incubation with an irrelevant antibody at high concentration, all as outlined in Materials and Methods. An example for the latter is presented in Fig. SA-c of the supplemental material. The very few gold granules recognizable in these controls were not associated with any of the structures otherwise labeled by specific antibodies used in this study (Fig. 3 and see below).

Further proof for specific antibody binding was obtained from quantitative Western blot analyses whenever wild-type cells could be compared with aliquots after silencing of the respective gene (see below for PtSyb10).

PtSyb8-1 and PtSyb9-2 are localized to small vesicles along the cytopharynx at the site of nascent food vacuole formation. We constructed N-terminal and C-terminal GFP fusions of PtSyb8-1. When expressed in *P. tetraurelia*, with both PtSyb8-1 GFP-constructs we observed a pronounced crescent-shaped staining at the cytopharynx at the site of nascent food vacuole formation (Fig. 4A and C, arrowheads). We also observed staining of the membrane of the nascent food vacuole that had just pinched off (Fig. 4A and C, arrows). There was also some staining of smaller vesicles with both constructs (Fig. 4A and C). The shape of the labeled structure at the cytopharynx was to some extent dynamic, as labeled details were moving whereas GFP staining was observed to persist for a while on the newly invaginated food vacuole (Fig. 4A, C, and E to G). Sometimes, trails of stained vesicles leading to the cytopharynx similar to the transport of small vesicles along microtubular ribbons described by Schroeder et al. (54) were observed (Fig. 4E to H). Therefore, the localization seen for the PtSyb8-1 GFP-constructs is compatible with a localization to small vesicles surrounding the cytopharynx (see EM localization results, below).

We also constructed an N-terminal GFP fusion of PtSyb9-2 as a representative of the PtSyb9 subfamily and expressed this in *P. tetraurelia* cells. The localization observed for GFP–PtSyb9-2 (Fig. 5A and C) was identical to that of the PtSyb8-1 GFP-constructs. We found a strong crescent-shaped staining at the cytopharynx (Fig. 5A and C, arrowheads) and of postoral fibers; however, we never observed staining with GFP–Syb9-2 on internalized food vacuoles.

Additionally, we tried to localize the endogenous proteins with specific antibodies. Polyclonal antibodies were raised against PtSyb8-$1_{1–205}$ and PtSyb9-$1_{1–195}$ and affinity purified against the denatured peptide used for immunization. In fixed and permeabilized cells, both antibodies showed strong staining along the lining of the oral cavity (Fig. 6A and C), but both antibodies also exhibited some staining of the cell surface. Outside these structures no consistent or significant staining of any details could be recognized (Fig. 6D). The anti-PtSyb9 antibody recognized the contractile vacuole systems only so slightly that this was hardly

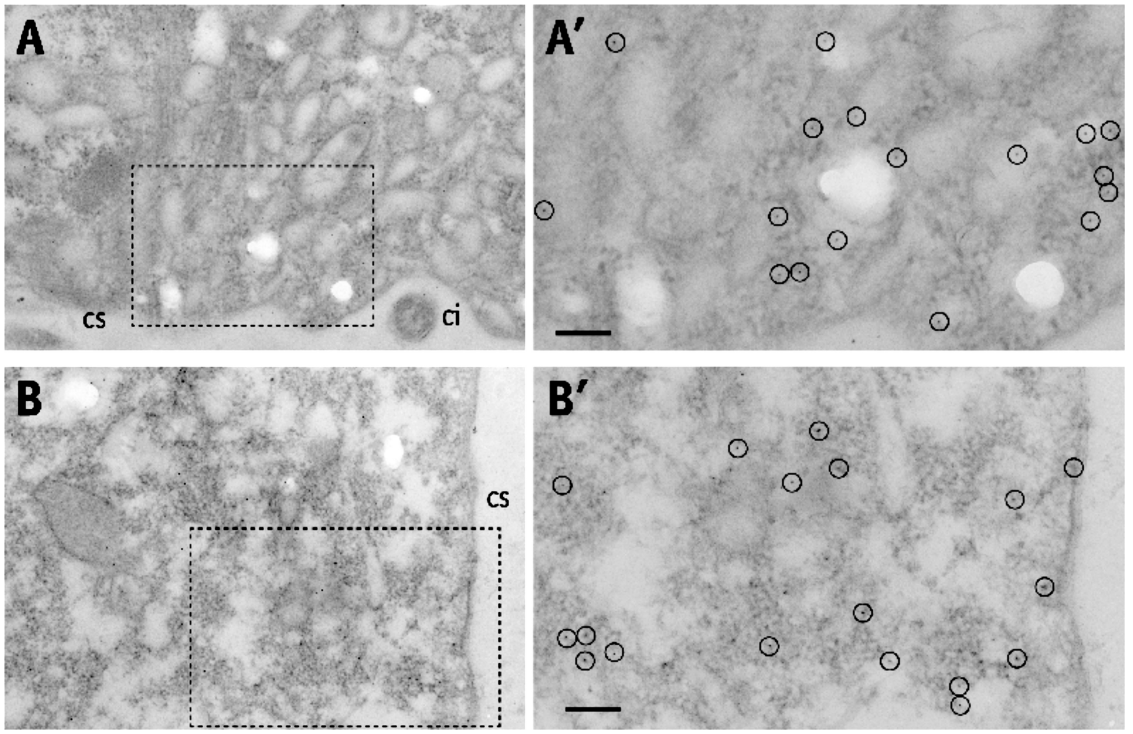

FIG. 7. EM localization of PtSyb8-1 and PtSyb9 to two morphologically different nonacidosomal vesicle populations near the cytostome. (A) Labeling of vesicles around the cytostome (cs) with anti-PtSyb8. ci, cilium. (A′) Enlargement from panel A, showing labeling with anti-PtSyb8 antibodies near small vesicles. (B) Labeling in the area of nascent food vacuole formation near the cytopharynx with anti-PtSyb9. (B′) Enlargement of panel B. Bars, 100 nm.

above background. Concomitantly, no staining of the contractile vacuole complex with the GFP-constructs was achieved.

To address the localization of PtSyb8 and PtSyb9 in more detail, we used the available anti-PtSyb8 and anti-PtSyb9 antibodies for immuno-EM studies. Labeling with anti-PtSyb8 was found closely associated with two types of ~100- to 200-nm large vesicles, one slightly elongate and the other one round, both surrounding the cytopharynx and both being different from acidosomes according to size (Fig. 7A and A′). Likewise, for PtSyb9 we found labeling of less regularly shaped vesicles with anti-PtSyb9 antibody in the vicinity of the cytopharynx in the region where the phagosome would form (Fig. 7B and B′). These EM localizations of PtSyb8-1 and PtSyb9-2 agree with the localizations observed at the light microscope level.

PtSyb10-1 is localized at the cell membrane close to basal bodies and also shows strong labeling of the oral cavity. We tried expressing N-terminal and C-terminal GFP fusions of PtSyb10-1 in *P. tetraurelia* cells. Unfortunately, an N-terminal fusion of PtSyb10-1 did not exit the endoplasmic reticulum, possibly due to masking of a sorting motif or misfolding caused by the GFP tag (data not shown; see comments in the Discussion). The C-terminal GFP fusion construct PtSyb10-1–GFP produced a staining of the cell surface and strong staining of the oral cavity (Fig. 8A and B). At the cell surface, some punctate or circular accumulations of staining were observed at higher magnification (Fig. 8A, inset). There was also some background staining inside the cell, but the cytoproct and macronucleus as well as food vacuoles were always devoid of staining. In fixed PtSyb10-1–GFP cells, the surface pattern became more prominent, particularly on surface ridges (Fig. 8C to E). While there is a general coincidence between live and fixed cells, minor differences have not been analyzed in any more detail.

We also raised a specific antibody against PtSyb10-1_{1-198}. Double staining with an anti-α-tubulin antibody revealed that PtSyb10 is localized in close apposition to basal bodies but not exactly overlapping with the anti-α-tubulin antibody labeling of the basal bodies (Fig. 9A). We also found staining at the dorsal and ventral sides of the oral cavity and some labeling on the contractile vacuole complexes (Fig. 9B). Three-dimensional (3D) rendering of confocal image stacks revealed prominent labeling of the cell cortex, particularly of the surface ridges (Fig. 9C), that was closely correlated with, but clearly distinct from, the anti-α-tubulin label (Fig. 9D).

In EM images obtained from PtSyb10-1–GFP–expressing cells we found immunogold labeling with an anti-GFP antibody of the cell membrane and outer alveolar sac membrane, but not on mitochondria or trichocysts (Fig. 10A, D, and E). In those cells we also found prominent clusters of label on the ciliary bases close to basal bodies and in the vicinity of alveolar sacs (Fig. 10B and C) that may correspond to the occasionally observed ring-shaped pattern observed in live GFP images (Fig. 8A, inset). A similar immunogold labeling of the cell membrane close to the ciliary bases was observed in the oral cavity (data not shown). These observations are compatible with the GFP and antibody fluorescence images (Fig. 8A and B and 9B). Similarly, ill-defined immunogold staining of domains between ER-containing regions (Fig. 10D and E) correlates with fluorescence microscopy results (Fig. 8B and 9B).

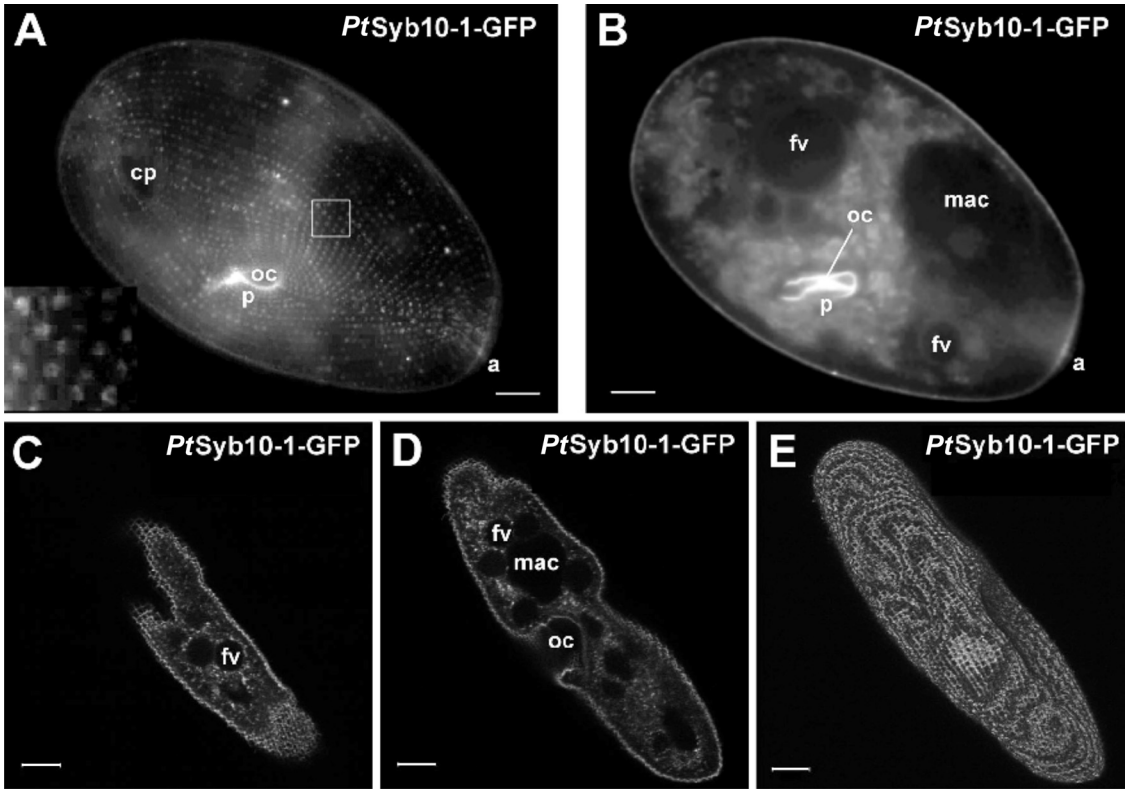

FIG. 8. (A and B) Surface (A) and median (B) focus of epifluorescence of a living cell expressing PtSyb10-1–GFP, showing punctate and partly circular (A, inset) surface staining with clear exclusion of the cytoproct (cp) and strong labeling lining the sides of the oral cavity (oc). The macronucleus (mac) and food vacuoles (fv) are free of label and clearly visible as dark exclusions of staining. a, anterior end of the cell; p, peniculus. (C to E) Confocal image slices (1 μm) of a fixed PtSyb10-1–GFP–expressing cell near the surface (C), a median plane (D), and a 3D reconstruction of the image stack (E), showing a regular pattern of surface ridges. Bars, 10 μm.

Functional aspects obtained from Pt*syb10* gene silencing. We silenced Pt*syb10* by using a construct containing sequences shared by both paralogs, PtSyb10-1 and PtSyb10-2, as outlined in Materials and Methods. We determined the lengths of cilia and normal forward swimming speed and rotations of cells along their path per unit time during ciliary reversal induced by depolarization by adding 10 mM KCl (Table 2), as defined in Materials and Methods. As controls we used either the empty vector, pPD, or this vector with an *nd7* silencing sequence (55). (Note that *nd7* is irrelevant for ciliary activity but allows easy control of successful silencing by the absence of a stimulated exocytotic response.) As shown in Table 2 we could find no effect of PtSyb10 silencing on either the length of cilia or on normal forward swimming. However, rotation frequency (number of rotations per second; determined as specified in Materials and Methods) during depolarization-induced ciliary beat reversal was reduced to 79% in PtSyb10-silenced cells, compared to the data obtained with the *nd7* construct, and to 62.5% compared to the empty vector control ($P = 0.01$ and 0.00002, respectively). No significant difference could be ascertained between the two controls ($P < 0.15$). PtSyb10 downregulation achieved by gene silencing (applying transformed food bacteria as described in Materials and Methods) was ascertained by Western blotting using tubulin as an invariant control (Fig. 11). In Western blot assays of PtSyb10-silenced cells, PtSyb10 was significantly downregulated to between 24 and 41% (Table 2). Thus, we found a partial PtSyb10 downregulation and in parallel a partial reduction of the response to depolarization.

NSF silencing discloses vesicles along the cell membrane. The rationale of these experiments was to stop vesicle fusion after delivery to the cell membrane by inhibiting the arrangement of SNAREs into fusion-competent complexes, a process that normally is mediated by the activity of the SNARE-specific chaperone NSF (see the introduction). As we have previously demonstrated, this approach is appropriate to pinpoint "cryptic" fusion sites, which are normally not seen by EM analysis because of the short time required for fusion (36). This approach aims not only at understanding in more detail the implications of PtSyb10 labeling around the basis of cilia but also at identifying any other sites of vesicle delivery. In fact, after silencing of NSF we could detect a large number of vesicle docking/fusion sites at the cell membrane on electron micrographs (Fig. 12A to D), whereas previously only the small areas of parasomal sacs have been considered appropriate for vesicle endocytosis and constitutive exocytosis (19).

In more detail, in the NSF-silenced cells we saw numerous vesicles between the alveolar sacs and the cell membrane (Fig. 12A and B) which looked like a disturbance of membrane delivery and/or turnover. Occasionally very small vesicles were recognizable (Fig. 12C and D), occasionally near a ciliary base (Fig. 12D). Note that no such vesicles were seen in controls (see Fig. SB in the supplemental material; see also the online

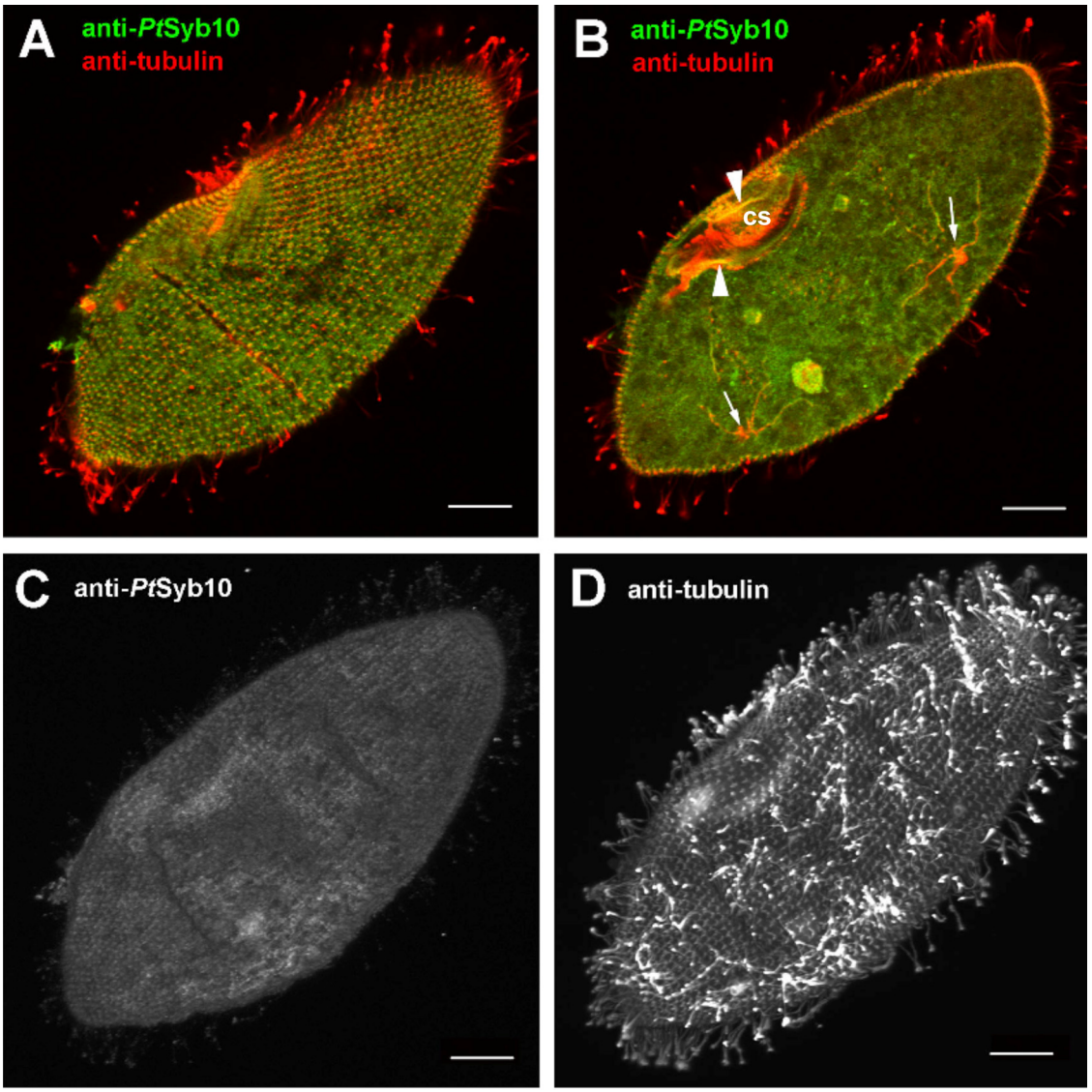

FIG. 9. Confocal images of double staining with a specific anti-PtSyb10 and an anti-α-tubulin antibody. (A) Surface slice showing close apposition but no exact overlap of anti-PtSyb10 and anti-α-tubulin staining of basal bodies. (B) Median slice showing strong staining with anti-α-tubulin but less with anti-PtSyb10 antibodies at the cytostome (cs) and cytopharynx, with some overlap along distinct microtubule arrays (arrowheads) and possibly some minor overlap of staining at the contractile vacuole systems (arrows). (C and D) 3D rendering of the anti-PtSyb10-1 label (C) and of the anti-α-tubulin label confocal image stacks (D), clearly showing different patterns. Also note staining of cilia with anti-tubulin but no labeling with anti-PtSyb10 antibodies in panels A, B, and C. Bars, 10 μm.

image series by R. D. Allen at http:/www5.pbrc.hawaii.edu /allen/). These data suggest that SNARE-mediated vesicle trafficking to the cell membrane may occur at different sites of the cell membrane, and also outside parasomal sacs.

Early endosomes (terminal cisternae) are labeled by GFP–PtSyb11-1. We constructed an N-terminal GFP-fusion construct of PtSyb11-1 and microinjected it into the macronucleus of *P. tetraurelia* cells. All successfully injected cells showed a regular punctate pattern just below the surface, which nicely agreed with the positioning of early endosomes (terminal cisternae). Additionally, we observed a faint staining of the plasma membrane and a strong line of label at one side of the cytostome (Fig. 13A and B). Occasionally, labeling of single food vacuoles with GFP–PtSyb11-1 was observed (Fig. 13B).

PtSyb12-1 lacks a transmembrane domain and occurs in the cytosol. Even though only the relationship to the PtSyb11 subfamily marks PtSyb12-1 as an R-SNARE, we tried to access its localization with a GFP-fusion construct. Not surprisingly, owing to its lack of a transmembrane domain, GFP–PtSyb12-1 was found in the cytosol (Fig. 13D and E), and also vaguely labeling of the surface ridges was found (Fig. 13D). As mentioned, it is questionable whether PtSyb12-1 is a SNARE protein at all.

DISCUSSION

We identified new synaptobrevin-like SNAREs in *Paramecium* and isolated the mRNAs for the subtypes indicated (Fig. 1; Table 1). Homology-based sequence analysis allowed us to identify

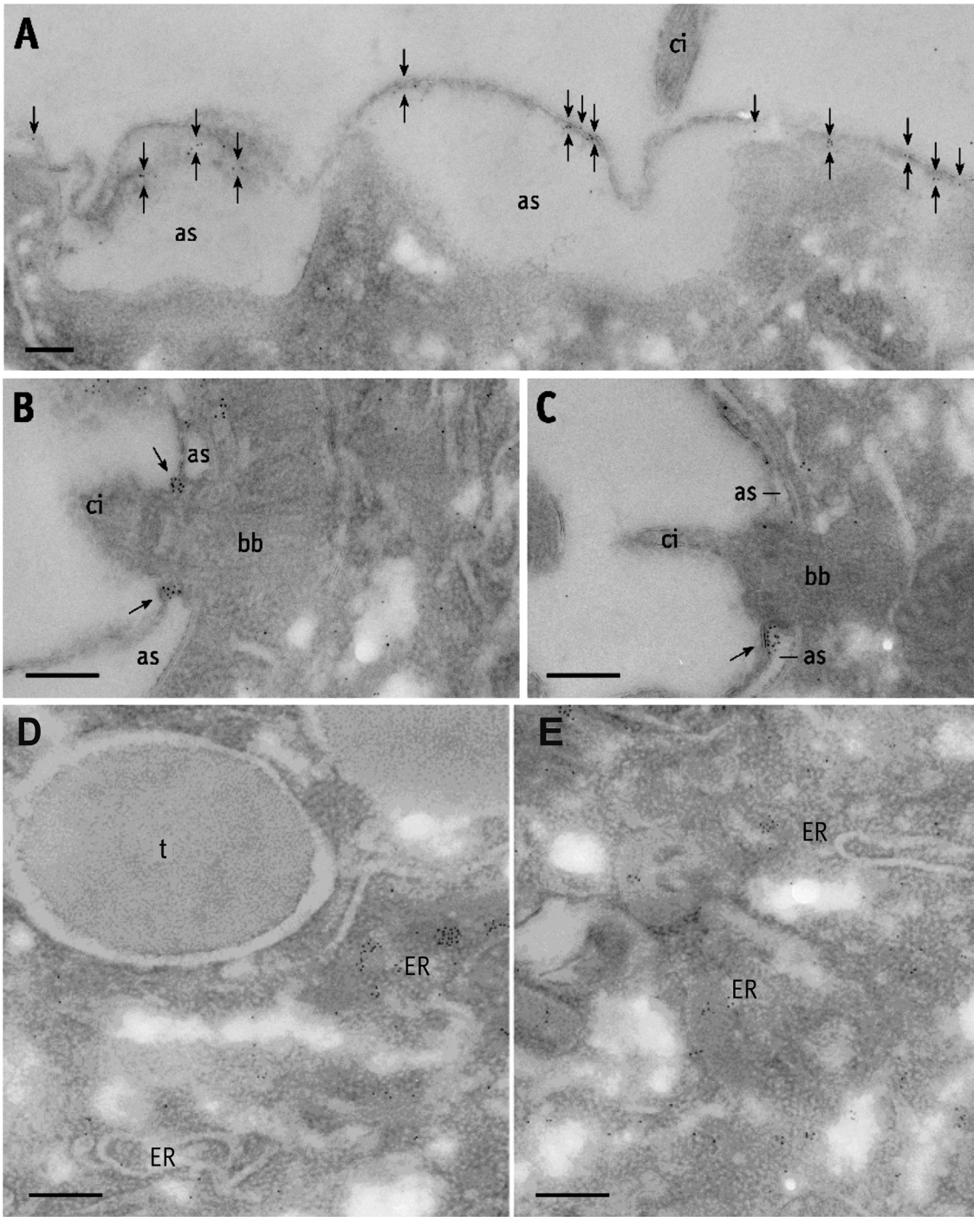

FIG. 10. Immuno-EM localization of PtSyb10-1–GFP detected with an anti-GFP antibody followed by protein A-Au_5. (A) Staining (arrows) of the complex formed by the plasma membrane and peripheral membrane of alveolar sacs (as). ci, cilium. (B and C) Strong labeling on both sides around a cilium at the site of cell membrane/cilium transition. (D and E) Only a small amount of label occurs inside the cytosolic compartment, without any clear correlation with subcellular compartments with the possible exception of the ER, while irrelevant structures such as trichocysts (t) are label free. bb, basal body. Bars, 250 nm.

these molecules as members of the synaptobrevin family, with the exception of PtSyb12 (see below). The newly described SNAREs and some other ones previously identified have been localized as GFP-fusion proteins and by antibodies at the light microscopy and EM levels, as summarized in Fig. 14, thus yielding important hints to their respective contributions to the elaborate vesicle trafficking system in *Paramecium*. More specifically, the functional significance of the "paraciliary" localization of PtSyb10 has been complemented by posttranscriptional homology-dependent gene silencing experiments.

TABLE 2. Effects of Pt*syb10* silencing on cilia and ciliary activity in *P. tetraurelia*

Parameter analyzed[a]	Relative value (%)[d] when indicated gene (group designation) was silenced (no of cells analyzed)			*P* value (groups compared)
	None[b] (A)	*nd7*[c] (B)	Pt*syb10* (C)	
Length of cilia	100 ± 3.6 (13)		96.6 ± 2.5 (19)	≤0.43[e] (A/C)
Normal forward swimming speed of cells		100 ± 3.8 (30)	95.2 ± 23.7 (30)	≤0.41[e] (B/C)
Rotations/s (performed by cells during swimming, KCl depolarization)	100.0 ± 6.6 (35)	100 ± 2.8 (15)	79.1 ± 4.5 (45) 62.5 ± 2.9 (65)	≤0.01 (B/C) ≤0.00002 (A/C) ≤0.15 (A/B)
Extent of PtSyb10 expression[f]	100		24.2–41.0	Highly significant

[a] For more details, see Materials and Methods.
[b] The empty pPD vector was applied for controls.
[c] The *nd7* gene is relevant for exocytosis but not for ciliary activity (see Results).
[d] For a better comparison, data for controls were normalized to 100%.
[e] Not a significant difference.
[f] Data obtained from quantitative evaluation of Western blots. The difference indicated for group A versus C, i.e., with and without Pt*syb10* silencing, shows that the intensity of the PtSyb10 band was reduced by a factor of ~2.5 to 4 due to silencing in the different evaluations indicated, while the intensity of the tubulin band remained practically identical (within ~5%) with and without Pt*syb10* silencing.

Comparison of the newly described SNAREs with those in other systems. Essential features are compiled in Table 1. With the exception of aberrant PtSyb12, discussed below, PtSyb8, PtSyb9, PtSyb10, and PtSyb11 all contain a carboxy-terminal transmembrane anchor preceded by a SNARE domain, whereas only PtSyb8 and PtSyb9 dispose of a longin domain. Such a longin domain has been recognized already in the previously described R-SNAREs (longins) of *Paramecium* (53), and it is typical of most plants (41), in contrast to the brevins found in most animal R-SNAREs (32). Another feature concerns the zero-layer amino acid, normally Arg (32). As already reported, some of the previously published PtSNAREs contain an aberrant amino acid in their zero layer (37, 53). However, deviations from the orthodox situation are not so infrequent in a variety of systems, from yeast to mammalian cells, and may eventually reduce SNARE complex stability and cause defects in membrane traffic (17, 24).

Localization of R-SNAREs, functional implications, and identification of new types. It became clear that the PtSyb4/5 group represents unusual SNAREs with no homologs outside the ciliates. We found this group of SNAREs associated with small vesicles that are not acidic. The PtSyb5-positive type is possibly related to trichocyst biogenesis for the following reasons. (i) These structures are not remarkably acidic (42), just like mature trichocysts and their precursor compartments (22). (ii) These structures look misshapen in the fluorescent images as well as in the electron micrographs, where gold label is intimately apposed to "free" (undocked) trichocysts with which they share the same structure typical of the trichocyst secretory materials. (iii) The labeled structures show striking similarity to the compartments observed as storage compartments during defective dense core vesicle processing in *Tetrahymena* (11) or in *Paramecium* (59). It may be that in our experiments this morphology is also due to missorting, in this case due to overexpression. Overexpression may, thus, render visible the long-sought-after trichocyst-specific R-SNARE that otherwise is too scarce to become visible.

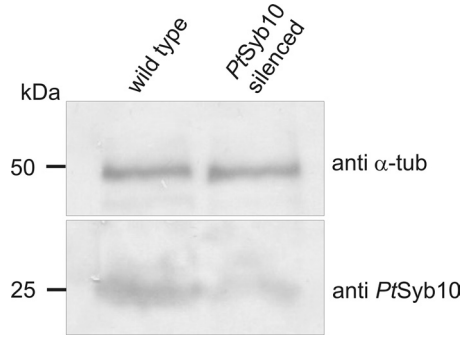

FIG. 11. Western blot of protein preparations from PtSyb10-silenced cells and wild-type cells. As a loading control, the same blot was probed with antibodies against α-tubulin (α-tub, upper panel) and showed very similar protein amounts (~ 20 ng) in both lanes. In extracts prepared from PtSyb10-silenced cells, antibodies against PtSyb10 (lower panel) recognized a significantly reduced amount of PtSyb10 antigen compared to wild-type cells.

Since homologs to the PtSyb4/5 group were only found in another ciliate, *Tetrahymena thermophila*, whose genome sequence is also publicly available, it is well possible that these aberrant synaptobrevin-like SNAREs have special functions, including trichocyst development in the case of PtSyb5. To ascertain this prediction, further investigation and functional tests will be required.

The subfamilies PtSyb8 to PtSyb12 are a group of R-SNAREs related to each other. Even though we found them on a variety of structures, all, with the exception of PtSyb12-1, showed some association with the cytostome. In agreement with this the SNARE-specific chaperone NSF was also found enriched at the cytostome and the cytoproct after treatment of carefully permeabilized cells with ATP-γ-S and NEM, which inhibits NSF function (36). In fact, these sites are places of intense vesicle trafficking (2, 3, 5). Our present work identifies a previously unexpected high number of different synaptobrevin-like SNAREs associated with the cytostome and cytopharynx. All those SNAREs that were analyzed at the EM level were localized on small vesicles in the vicinity of the cytostome.

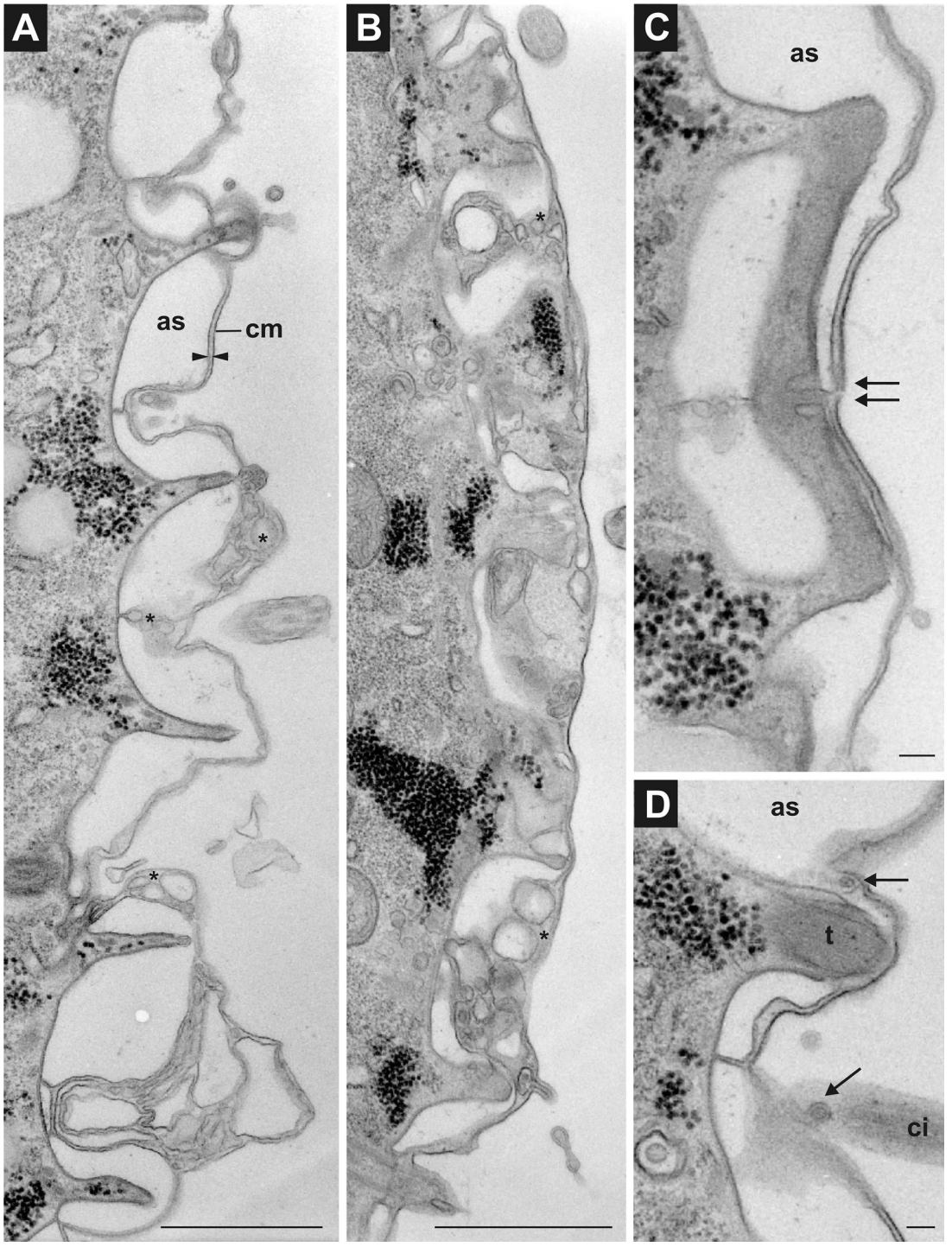

FIG. 12. Examples of ultrastructural changes observed in the *Paramecium* cortex after Pt*NSF* silencing. Note that the normally thin complex made by the cell membrane (cm) and the outer membrane of alveolar sacs (as), as seen at the arrowheads, is frequently interrupted by membrane-bounded structures of different sizes (asterisks) that may occasionally appear as very distinct small vesicles (arrows in panels C and D), e.g., at the base of cilia (ci in panel D). No comparable small vesicles associated with the surface membrane were seen in non-NSF-silenced cells, as discussed in the text. t, trichocyst. Bars, 1 μm (A and B) or 0.1 μm (C and D).

There seems to be a surprising level of functional differentiation at the molecular level of those morphologically similar small vesicles. Their shape varies from round to slightly elongate and they are smaller (~0.1 to 0.2 μm) (Fig. 7A′ and B′) than acidosomes (~0.8 μm) (2, 3, 20). It is well possible that the observed differences in localization, i.e., along the peniculus, at the cytopharynx and on nascent food vacuoles, on early endosomes, and on trails of vesicles along microtubules ema-

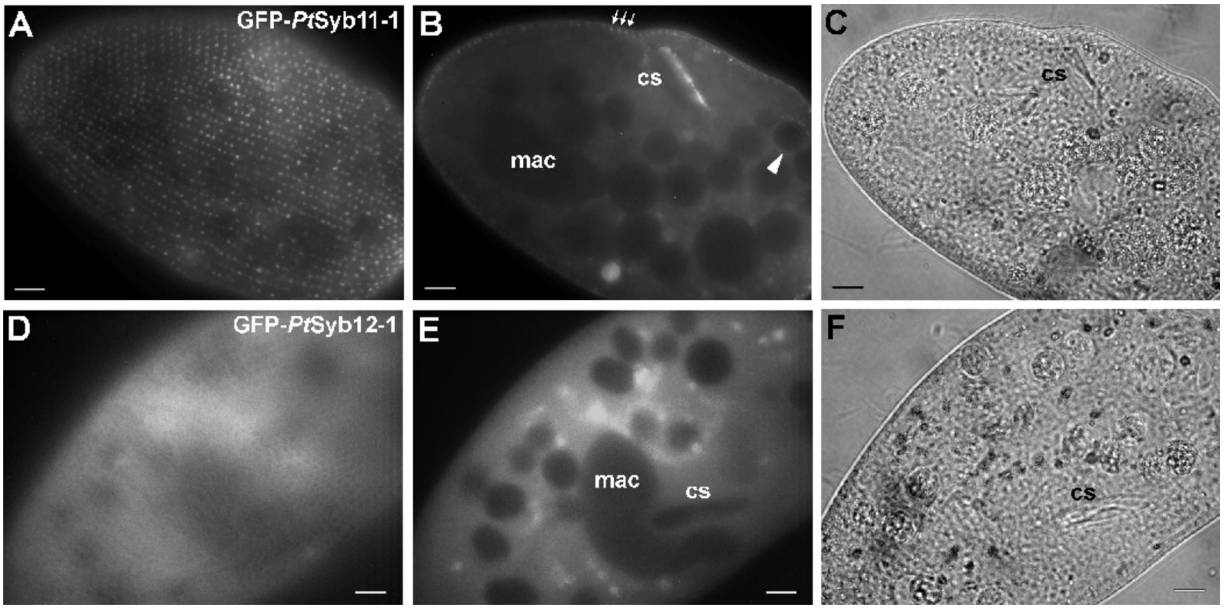

FIG. 13. Localization of GFP–PtSyb11-1 and GFP–PtSyb12-1. (A and B) Surface (A) and median (B) focus of epifluorescence of a living cell expressing GFP–PtSyb11-1. The regular punctate pattern is due to staining of regularly arranged terminal cisternae (early endosomes), situated below ciliary basal bodies, ~1 μm below the cell surface (arrows). There was little staining of the cell membrane or of a food vacuole (arrowhead) visible in panel B, and strong staining occurred only at one side of the cytostome (cs). (C) Corresponding bright-field image. (D and E) Surface (D) and median (E) focus of epifluorescence of a living cell expressing GFP–PtSyb12-1, which largely appears soluble in the cytosol. Also, some faint staining of "surface ridges," of the egg case-like cell surface, is observed in panel D. (E) Cytostome (cs), food vacuoles, and the macronucleus (mac) are devoid of label, while some label appears clustered in the cytosolic compartment. (F) Corresponding bright-field image. Bars, 10 μm.

nating from the cytopharynx, represent different stages of maturation and recycling of these small vesicles (2, 3, 5) during which synaptobrevin-like SNAREs are exchanged.

The cell surface staining pattern of PtSyb11 (Fig. 13A) fits well with staining of early endosomes (terminal cisternae). These are located proximal of each basal body of a cilium, and concomitantly the fluorescence staining is located clearly below the cell surface. This corresponds to a correlated immunofluorescence and immuno-EM analysis of some other membrane components (61). The staining of the cytostome is identical to that found with PtSyx3-1–GFP (37).

Aberrant types. PtVAMP741 was not further investigated in this study and, in our opinion, may represent an artificial pseudogene. This assumption is supported by our failure to amplify any Pt*VAMP741* RT-PCR product from cDNA.

One of the more distantly related proteins of this study,

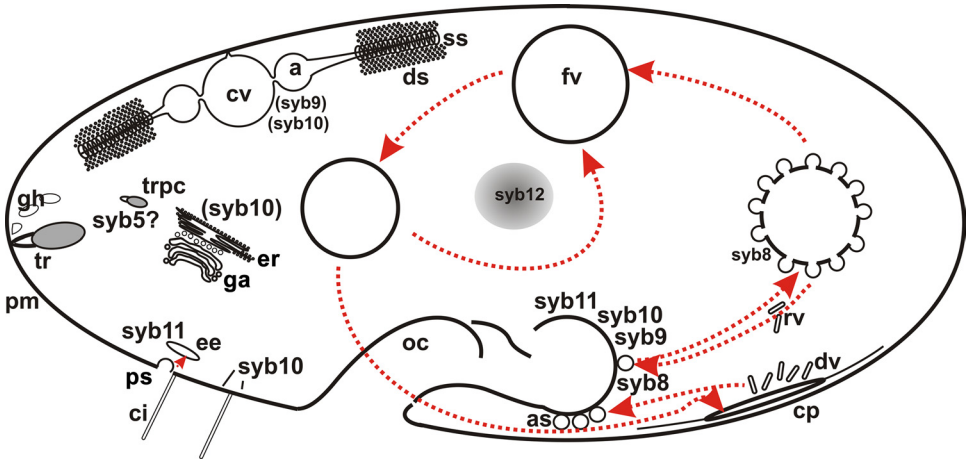

FIG. 14. Scheme of a *Paramecium* cell superimposed with immunolocalization and GFP localization of the PtSNAREs that we worked with in this study. The trafficking scheme is based on references 4, 20, and 47. The scheme contains elements of the osmoregulatory system (a, ampulla; cv, contractile vacuole; ds, decorated spongiome; ss, smooth spongiome), of the phagosomal apparatus (as, acidosomes mediating acidification of a food vacuole [fv] after pinching off; cp, cytoproct [defecation site]). ci, cilia; dv, discoidal vesicles and other recycling vesicles (rv); ee, early endosomes; er, endoplasmic reticulum; ga, Golgi apparatus; gh, ghosts (from released trichocysts); oc, oral cavity; pm, plasma membrane; ps, parasomal sacs; tr, trichocysts; trpc, trichocyst precursor.

PtSyb12-1, probably does not represent a member of the SNARE protein family, because it lacks both a discernible SNARE motif and a transmembrane domain and we did not find it associated with membrane-bound structures in the *Paramecium* cells.

Implications of PtSyb10 near ciliary bases. Interestingly, one of the SNAREs investigated here, PtSyb10-1, showed a close association with the ciliary bases (and some additional sites). If expressed with GFP at the C terminus, localization was cortical, as with antibodies, while GFP attached to the N terminus inhibited exit from the endoplasmic reticulum. This discrepancy may be reconciled by the relevance of the folding state of the N-terminal half for exit from the endoplasmic reticulum and further targeting, as found, e.g., with Sec22 in other eukaryotic cells (44).

It appears feasible that PtSyb10-1 could be involved in vesicle trafficking by delivering components, e.g., for formation and maintenance of the cilia and/or of their functions, including the nearby somatic (nonciliary) cell membrane. Data available on SNAREs in cilia are very rare and mainly concern the rod outer segment (13), where Syx3 remains excluded from the membrane of this ciliary derivative (10). An additional question is why a v-SNARE can be enriched in the cell membrane. In fact, a similar situation is reported from nerve terminals in *Caenorhabditis elegans* (15), probably as a result of intense membrane delivery and only partial retrieval of the v-SNARE. Another explanation of PtSyb10 clusters near ciliary bases would be that SNAREs can also serve the formation of specialized domains for signaling, for example (see below).

Considering the limited space for vesicle delivery at the *Paramecium* cell surface, which is largely occupied by alveolar sacs, docked trichocysts, and ciliary basal bodies, scientists have tacitly agreed up to now that "parasomal sacs" (~100 nm in diameter, strictly arranged as puncta near ciliary bases) would be the only sites accessible for vesicles, i.e., clathrin-mediated endocytosis and vesicle delivery for membrane turnover/biogenesis (12, 19). However, we now report an annular PtSyb10 labeling around ciliary bases (Fig. 8A and 10B and C). Consequently, we asked whether vesicles are seen outside the established sites of parasomal sacs. This was the rationale of the NSF silencing experiments, which allow "freezing" vesicles in a position ready for fusion and EM analysis (36). This approach clearly revealed many vesicle-cell membrane interactions, some of the vesicles being very small (~50 to 100 nm), over large parts of the cell surface (Fig. 12C and D). Normally, because of the transient nature of docking and membrane fusion, such vesicles may not be recognized outside parasomal sacs (see Fig. SB in the supplmental material), as repeatedly documented in the *Paramecium* literature and in the comprehensive online image series by R. D. Allen (see http:/www5.pbrc.hawaii.edu/allen/).

From the localization of PtSyb10 in "paraciliary" small domains one cannot necessarily derive its engagement in ciliary biogenesis, as its function may be indirect. Ciliary activity, e.g., depolarization-induced ciliary reversal, depends not only on the ciliary voltage-dependent Ca^{2+} channels but also on K^+ efflux channels in the somatic membrane (40, 43). In the *Paramecium pawn-B* mutant, a defective transcript of a Ca^{2+} channel modulator is delivered only to near the cell surface and, thus, causes malfunction (29). Furthermore, some voltage-dependent cation channels are associated with specific SNAREs in higher eukaryotic cells (26). These situations may be the basis of the observations we made after PtSyb10 silencing, whereby the depolarization-induced ciliary reversal was significantly slowed down. However, for the time being we have to leave open the precise implications of the small paraciliary PtSyb10 domains, although the phenotype achieved by silencing is clear.

Conclusions. We assume that the present contribution may rather safely complete the number of SNARE genes occurring in *Paramecium*. Based on data mining in the *P. tetraurelia* genome database, combined with experimental analysis, we can now estimate the approximate number of synaptobrevin-like SNAREs as ~20, although some of them have quite aberrant features (Fig. 1) and, thus, may not be functional. Our present work gives additional support to the conclusion by Fasshauer and colleagues that "it seems likely that the more complex membrane trafficking pathways of *Paramecium* are built on the basic subcellular organization known from 'typical' eukarytotic cells" (39). Although the generally low level of sequence conservation among SNAREs and the huge evolutionary distances of ciliates to metazoans make it difficult to predict SNARE proteins with certainty, we were able to assign newly identified SNAREs in *P. tetraurelia* cells mainly to the sites of the most intense vesicle trafficking, i.e., along the endo-/phagocytotic route. Remarkably, the localization of several SNAREs may overlap at these sites. This may indicate an even higher level of functional specialization than recognized up to now. On this background it no longer appears surprising that a *Paramecium* cell contains a large number of SNAREs equivalent to that found in higher plants (41) and humans (39).

ACKNOWLEDGMENTS

We thank D. Fasshauer and R. Jahn (Max-Planck-Institute for Biophysical Chemistry, Göttingen, Germany) for access to the server with the SNARE database and identification of some new SNARE proteins in *P. tetraurelia*. At Konstanz University we thank E. May for access to the LSM510 Meta confocal microscope, E. Ladenburger for help with Western blot analyses, L. Nejedli for preparing EM samples, J. Hentschel and D. Bliestle for electronic image processing, and R. Vögele for the gift of the pRV11 expression vector.

This work was supported by the Deutsche Forschungsgemeinschaft (grant PL 78/20-3 to H.P.).

REFERENCES

1. **Adoutte, A., P. Delgado, A. Fleury, N. Levilliers, M. C. Laine, M. C. Marty, E. Boisvieux-Ulrich, and D. Sandoz.** 1991. Microtubule diversity in ciliated cells: evidence for its generation by post-translational modification in the axonemes of Paramecium and quail oviduct cells. Biol. Cell **71:**227–245.
2. **Allen, R. D.** 1984. *Paramecium* phagosome membrane: from oral region to cytoproct and back again. J. Protozool. **31:**1–6.
3. **Allen, R. D., and A. K. Fok.** 1993. Endosomal membrane traffic of ciliates, p. 57–83. *In* H. Plattner (ed.), Advances in cell and molecular biology of membranes. JAI Press, Greenwich, CT.
4. **Allen, R. D., and A. K. Fok.** 2000. Membrane trafficking and processing in Paramecium. Int. Rev. Cytol. **198:**277–318.
5. **Allen, R. D., and L. A. Staehelin.** 1981. Digestive system membranes: freeze-fracture evidence for differentiation and flow in *Paramecium*. J. Cell Biol. **89:**9–20.
6. **Altschul, S. F., T. L. Madden, A. A. Schaffer, J. Zhang, Z. Zhang, W. Miller, and D. J. Lipman.** 1997. Gapped BLAST and PSI-BLAST: a new generation of protein database search programs. Nucleic Acids Res. **25:**3389–3402.
7. **Antonin, W., D. Fasshauer, S. Becker, R. Jahn, and T. R. Schneider.** 2002. Crystal structure of the endosomal SNARE complex reveals common structural principles of all SNAREs. Nat. Struct. Biol. **9:**107–111.
8. **Aury, J. M., O. Jaillon, L. Duret, B. Noel, C. Jubin, B. M. Porcel, B. Ségurens, V. Daubin, V. Anthouard, N. Aiach, O. Arnaiz, A. Billaut, J.**

Beisson, I. Blanc, K. Bouhouche, F. Câmara, S. Duharcourt, R. Guigo, D. Gogendeau, M. Katinka, A. M. Keller, R. Kissmehl, C. Klotz, F. Koll, M. A. Le, G. Lepère, S. Malinsky, M. Nowacki, J. K. Nowak, H. Plattner, J. Poulain, F. Ruiz, V. Serrano, M. Zagulski, P. Dessen, M. Bétermier, J. Weissenbach, C. Scarpelli, V. Schächter, L. Sperling, E. Meyer, J. Cohen, and P. Wincker. 2006. Global trends of whole-genome duplications revealed by the ciliate *Paramecium tetraurelia*. Nature **444:**171–178.

9. **Bairoch, A., P. Bucher, and K. Hofmann.** 1997. The PROSITE database, its status in 1997. Nucleic Acids Res. **25:**217–221.
10. **Baker, S. A., M. Haeri, P. Yoo, S. M. Gospe III, N. P. Skiba, B. E. Knox, and V. Y. Arshavsky.** 2008. The outer segment serves as a default destination for the trafficking of membrane proteins in photoreceptors. J. Cell Biol. **183:** 485–498.
11. **Bowman, G. R., and A. P. Turkewitz.** 2001. Analysis of a mutant exhibiting conditional sorting to dense core secretory granules in *Tetrahymena thermophila*. Genetics **159:**1605–1616.
12. **Capdeville, Y.** 2000. *Paramecium* GPI proteins: variability of expression and localization. Protist **151:**161–169.
13. **Chuang, J. Z., Y. Zhao, and C. H. Sung.** 2007. SARA-regulated vesicular targeting underlies formation of the light-sensing organelle in mammalian rods. Cell **130:**535–547.
14. **Dillon, P. J., and C. A. Rosen.** 1993. Use of polymerase chain reaction for the rapid construction of synthetic genes. Methods Mol. Biol. **15:**263–269.
15. **Dittman, J. S., and J. M. Kaplan.** 2006. Factors regulating the abundance and localization of synaptobrevin in the plasma membrane. Proc. Natl. Acad. Sci. U. S. A. **103:**11399–11404.
16. **Dryl, S.** 1959. Effect of adaptation to the environment on chemotaxis of *Paramecium caudatum*. Acta Biol. Exp. **19:**83–93.
17. **Fasshauer, D., R. B. Sutton, A. T. Brunger, and R. Jahn.** 1998. Conserved structural features of the synaptic fusion complex: SNARE proteins reclassified as Q- and R-SNAREs. Proc. Natl. Acad. Sci. U. S. A. **95:**15781–15786.
18. **Filippini, F., V. Rossi, T. Galli, A. Budillon, M. D'Urso, and M. D'Esposito.** 2001. Longins: a new evolutionary conserved VAMP family sharing a novel SNARE domain. Trends Biochem. Sci. **26:**407–409.
19. **Flötenmeyer, M., M. Momayezi, and H. Plattner.** 1999. Immunolabeling analysis of biosynthetic and degradative pathways of cell surface components (glycocalyx) in *Paramecium* cells. Eur. J. Cell Biol. **78:**67–77.
20. **Fok, A. K., and R. D. Allen.** 1993. Membrane flow in the digestive cycle of *Paramecium*, p. 85–111. *In* H. Plattner (ed.), Advances in biochemistry and biology of membranes. JAI Press, Greenwich, CT.
21. **Galvani, A., and L. Sperling.** 2002. RNA interference by feeding in *Paramecium*. Trends Genet. **18:**11–12.
22. **Garreau de Loubresse, N., M. C. Gautier, and L. Sperling.** 1994. Immature secretory granules are not acidic in *Paramecium* cells: implications for sorting to the regulated pathway. Biol. Cell **82:**139–147.
23. **Godiska, R., K. J. Aufderheide, D. Gilley, P. Hendrie, T. Fitzwater, L. B. Preer, B. Polisky, and J. R. Preer, Jr.** 1987. Transformation of *Paramecium* by microinjection of a cloned serotype gene. Proc. Natl. Acad. Sci. U. S. A. **84:**7590–7594.
24. **Graf, C. T., D. Riedel, H. D. Schmitt, and R. Jahn.** 2005. Identification of functionally interacting SNAREs by using complementary substitutions in the conserved 0′ layer. Mol. Biol. Cell **16:**2263–2274.
25. **Gurkan, C., A. V. Koulov, and W. E. Balch.** 2007. An evolutionary perspective on eukaryotic membrane trafficking. Adv. Exp. Med. Biol. **607:**73–83.
26. **Hagalili, Y., N. Bachnoff, and D. Atlas.** 2008. The voltage-gated Ca^{2+} channel is the Ca^{2+} sensor protein of secretion. Biochemistry **47:**13822–13830.
27. **Hauser, K., W. J. Haynes, C. Kung, H. Plattner, and R. Kissmehl.** 2000. Expression of the green fluorescent protein in *Paramecium tetraurelia*. Eur. J. Cell Biol. **79:**144–149.
28. **Hausmann, K., A. K. Fok, and R. D. Allen.** 1988. Immunocytochemical analysis of trichocyst structure and development in *Paramecium*. J. Ultrastruct. Mol. Struct. Res. **99:**213–225.
29. **Haynes, W. J., K. Y. Ling, R. R. Preston, Y. Saimi, and C. Kung.** 2000. The cloning and molecular analysis of pawn-B in *Paramecium tetraurelia*. Genetics **155:**1105–1117.
30. **Haynes, W. J., K. Y. Ling, Y. Saimi, and C. Kung.** 1995. Induction of antibiotic resistance in *Paramecium tetraurelia* by the bacterial gene APH-3′-II. J. Eukaryot. Microbiol. **42:**83–91.
31. **Haynes, W. J., B. Vaillant, R. R. Preston, Y. Saimi, and C. Kung.** 1998. The cloning by complementation of the pawn-A gene in *Paramecium*. Genetics **149:**947–957.
32. **Jahn, R., and R. H. Scheller.** 2006. SNAREs: engines for membrane fusion. Nat. Rev. Mol. Cell Biol. **7:**631–643.
33. **Jones, D. T.** 1998. Do transmembrane protein superfolds exist? FEBS Lett. **423:**281–285.
34. **Jones, D. T.** 1999. Protein secondary structure prediction based on position-specific scoring matrices. J. Mol. Biol. **292:**195–202.
35. **Jones, D. T., W. R. Taylor, and J. M. Thornton.** 1994. A model recognition approach to the prediction of all-helical membrane protein structure and topology. Biochemistry **33:**3038–3049.
36. **Kissmehl, R., M. Froissard, H. Plattner, M. Momayezi, and J. Cohen.** 2002. NSF regulates membrane traffic along multiple pathways in *Paramecium*. J. Cell Sci. **115:**3935–3946.
37. **Kissmehl, R., C. Schilde, T. Wassmer, C. Danzer, K. Nuehse, K. Lutter, and H. Plattner.** 2007. Molecular identification of 26 syntaxin genes and their assignment to the different trafficking pathways in *Paramecium*. Traffic **8:**523–542.
38. **Kissmehl, R., I. M. Sehring, E. Wagner, and H. Plattner.** 2004. Immunolocalization of actin in *Paramecium* cells. J. Histochem. Cytochem. **52:**1543–1559.
39. **Kloepper, T. H., C. N. Kienle, and D. Fasshauer.** 2007. An elaborate classification of SNARE proteins sheds light on the conservation of the eukaryotic endomembrane system. Mol. Biol. Cell **18:**3463–3471.
40. **Kung, C., and Y. Saimi.** 1982. The physiological basis of taxes in *Paramecium*. Annu. Rev. Physiol. **44:**519–534.
41. **Lipka, V., C. Kwon, and R. Panstruga.** 2007. SNARE-ware: the role of SNARE-domain proteins in plant biology. Annu. Rev. Cell Dev. Biol. **23:** 147–174.
42. **Lumpert, C. J., R. Glas-Albrecht, E. Eisenmann, and H. Plattner.** 1992. Secretory organelles of Paramecium cells (trichocysts) are not remarkably acidic compartments. J. Histochem. Cytochem. **40:**153–160.
43. **Machemer, H.** 1988. Electrophysiology, p. 185–215. *In* H. D. Görtz (ed.), *Paramecium*. Springer, Berlin, Germany.
44. **Mancias, J. D., and J. Goldberg.** 2007. The transport signal on Sec22 for packaging into COPII-coated vesicles is a conformational epitope. Mol. Cell **26:**403–414.
45. **McGuffin, L. J., K. Bryson, and D. T. Jones.** 2000. The PSIPRED protein structure prediction server. Bioinformatics **16:**404–405.
46. **Plattner, H.** 2002. My favorite cell: *Paramecium*. Bioessays **24:**649–658.
47. **Plattner, H., and R. Kissmehl.** 2003. Molecular aspects of membrane trafficking in *Paramecium*. Int. Rev. Cytol. **232:**185–216.
48. **Radek, R., and K. Hausmann.** 1996. Phagotrophy of ciliates, p. 197–219. *In* K. Hausmann and P. C. Bradbury (ed.), Ciliates: cells as organisms. G. Fischer, Stuttgart, Germany.
49. **Rossi, V., D. K. Banfield, M. Vacca, L. E. Dietrich, C. Ungermann, M. D'Esposito, T. Galli, and F. Filippini.** 2004. Longins and their longin domains: regulated SNAREs and multifunctional SNARE regulators. Trends Biochem. Sci. **29:**682–688.
50. **Rossi, V., R. Picco, M. Vacca, M. D'Esposito, M. D'Urso, T. Galli, and F. Filippini.** 2004. VAMP subfamilies identified by specific R-SNARE motifs. Biol. Cell **96:**251–256.
51. **Sambrook, J., E. Fritch, and T. Maniatis.** 1989. Molecular cloning: a laboratory manual. Cold Spring Harbor Laboratory Press, Cold Spring Harbor, NY.
52. **Schilde, C., K. Lutter, R. Kissmehl, and H. Plattner.** 2008. Molecular identification of a SNAP-25-like SNARE protein in *Paramecium*. Eukaryot. Cell **7:**1387–1402.
53. **Schilde, C., T. Wassmer, J. Mansfeld, H. Plattner, and R. Kissmehl.** 2006. A multigene family encoding R-SNAREs in the ciliate *Paramecium tetraurelia*. Traffic **7:**440–455.
54. **Schroeder, C. C., A. K. Fok, and R. D. Allen.** 1990. Vesicle transport along microtubular ribbons and isolation of cytoplasmic dynein from *Paramecium*. J. Cell Biol. **111:**2553–2562.
55. **Skouri, F., and J. Cohen.** 1997. Genetic approach to regulated exocytosis using functional complementation in *Paramecium*: identification of the ND7 gene required for membrane fusion. Mol. Biol. Cell **8:**1063–1071.
56. **Sonneborn, T. M.** 1974. *Paramecium aurelia*, p. 469–594. *In* R. C. Kung (ed.), Handbook of genetics. Plenum Press, New York, NY.
57. **Sutton, R. B., D. Fasshauer, R. Jahn, and A. T. Brunger.** 1998. Crystal structure of a SNARE complex involved in synaptic exocytosis at 2.4 Å resolution. Nature **395:**347–353.
58. **Timmons, L., D. L. Court, and A. Fire.** 2001. Ingestion of bacterially expressed dsRNAs can produce specific and potent genetic interference in *Caenorhabditis elegans*. Gene **263:**103–112.
59. **Vayssié, L., N. Garreau de Loubresse, and L. Sperling.** 2001. Growth and form of secretory granules involves stepwise assembly but not differential sorting of a family of secretory proteins in *Paramecium*. J. Cell Sci. **114:**875–886.
60. **Wassmer, T., M. Froissard, H. Plattner, R. Kissmehl, and J. Cohen.** 2005. The vacuolar proton-ATPase plays a major role in several membrane-bounded organelles in *Paramecium*. J. Cell Sci. **118:**2813–2825.
61. **Wassmer, T., R. Kissmehl, J. Cohen, and H. Plattner.** 2006. Seventeen α-subunit isoforms of *Paramecium* V-ATPase provide high specialization in localization and function. Mol. Biol. Cell **17:**917–930.
62. **Wirsel, S. G. R., R. V. Vögele, R. Bänninger, and K. W. Mentgen.** 2004. Cloning of β-tubulin and succinate dehydrogenase genes from *Uromyces fabae* and establishing selection conditions for their use in transformation. Eur. J. Plant Pathol. **110:**767–777.
63. **Zwilling, D., A. Cypionka, W. H. Pohl, D. Fasshauer, P. J. Walla, M. C. Wahl, and R. Jahn.** 2007. Early endosomal SNAREs form a structurally conserved SNARE complex and fuse liposomes with multiple topologies. EMBO J. **26:**9–18.